4. K_i, V_T, and k_{loss} were estimated from simulated TACs by Gjedde-Patlak, Logan, and Kumakura method.
5. We estimated the sensitivity of macro parameters to changes in dopamine synthesis, storage, and metabolism.

Detailed FDOPA kinetic model (DF model)

The compartment model used in TAC simulations of our study, DF model, is based on the biochemical pathways of dopamine as shown in Figure 1 (Cooper et al., 2003; Cumming et al., 1987; Firnau et al., 1987). DF model (Matsubara et al., 2010) describes dopamine synthesis [compartment "FDA(free)" and rate constant k_3], storage [compartment "FDA(-stored)" and rate constant k_7] and dopamine metabolism to its diffusible metabolites, [^{18}F]FDOPAC and [^{18}F]FHVA (compartment "FDOPAC," "FHVA," and rate constant, k_9^{dopac}, k_9^{hva}) (see Fig. 2). A set of differential equations to describe the exchange processes between compartments are derived such as general compartment model.

Acquisition of standard data as normal condition

An [^{18}F]FDOPA PET scan in a normal monkey was performed to obtain a control striatal TAC and metabolite-corrected arterial input function.

Animal procedures

A normal cynomolgus monkey (macaca fascicularis, body weight: 3.8 kg) was anesthetized by ketamine (8.4 mg, intramuscularly) and xylazine (1.7 mg, intramuscularly) 3 h before the start of the scan. Propofol (6 mg/kg/h) and vecuronium (0.02 mg/kg/h) was also infused continuously. For the inhibition of the peripheral metabolism of [^{18}F]FDOPA, carbidopa [5 mg/kg, i. v. (Chan et al., 1995; Cumming and Gjedde, 1998)] was administered 1 h before the injection of [^{18}F]FDOPA. The study protocol was approved by the Subcommittee for Laboratory Animal Welfare of the National Cardiovascular Center.

Scanning procedure

A PET scan was performed by PCA-2000A positron scanner (Toshiba Medical Systems Corporation, Tochigi, Japan. Spatial resolution: 6.2 mm, axial FOV: 162 mm), which was manufactured by OEM of Siemens ECAT ACCEL (Herzog et al., 2004). A transmission scan with a 3-rod source of ^{68}Ge-^{68}Ga was carried out for 15 min for attenuation correction 1 h before the [^{18}F]FDOPA injection. A 2D dynamic emission scan of 120 min duration with 45 frames (10 s × 18, 30 s × 6, 120 s × 7, 300 s × 8, 600 s × 6 frames), was initiated upon intravenous injection of [^{18}F]FDOPA (102 MBq).

Data processing

Data were corrected for scattered and attenuated photons and reconstructed by 2D direct-inversion Fourier transform (DIFT) algorithm (Herzog et al., 2004; Stark et al., 1981) with 3 mm FWHM Gaussian filter. ROIs were defined manually over the striatum and cerebellum for PET images, and TAC in these regions were obtained.

Acquisition for input function

For continuous measurement of the arterial input function, the radioactivity in the artery was measured by γ ray detector with GSO crystal (Kudomi et al., 2003) and a shunt line inserted between the artery and vein of the monkey. In addition, the arterial blood was sampled at 3, 10, 30, 60, 120 min after injection of [^{18}F]FDOPA for the correction of radiotracer in hemocyte and radiolabeled metabolites. The radioactivity of whole blood and supernatant of the centrifuged samples were measured by well counter (BeWell QS01A, Molecular Imaging Laboratory, Osaka, Japan) for acquisition of whole blood and plasma radioactivity, 0.6 ml of supernatant of sample at 10, 60, and 120 min was deproteinized as described previously (Cumming et al., 1999). The fraction for [^{18}F]FDOPA and [^{18}F]OMFD in these supernatants were measured with high-performance liquid chromatography (HPLC) with a C-18 reverse phase column and a flow through γ detector(BeWell QS01B, Molecular Imaging Laboratory, Osaka, Japan).

The arterial input function obtained by continuous measurement was corrected for the plasma fraction. Input functions for [^{18}F]FDOPA and [^{18}F]OMFD were calculated from plasma activity and fraction for radiolabeled metabolite with bi-exponential function (Takikawa et al., 1994), derived from the [^{18}F]FDOPA fraction measured by HPLC.

Simulation for TAC

In all simulations by DF model, total radioactivity was calculated by solving the differential equations using a four-dimensional Runge-Kutta algorithm as previous study (Matsubara et al., 2010). The definition of kinetic terms and concentration in the following equation is described in Table II. K_1^M and k_2^M, estimated by compartmental model analysis in cerebellum TAC as described in the previous study (Kumakura et al., 2005), were given in TAC simulation. For definition of K_1^D, k_2^D, k_3, and V_b, compartmental analysis with the model including k_{loss} (Wahl and Nahmias, 1996) was applied to a monkey striatal

TABLE II. Definitions of kinetic term in DF model

Terms	Units	Definition
K_1	g/ml/min	Rate constant for influx of tracer to tissue across Blood-Brain Barrier (BBB). K_1^D for FDOPA and K_1^M for OMFD.
k_2	min^{-1}	Rate constant for diffusion of tracer from tissue to plasma. k_2^D for FDOPA and k_2^M for OMFD.
k_3	min^{-1}	Rate constant for the activity of DOPA decarboxylase, the enzyme for the decarboxylation from FDOPA to FDA.
k_5	min^{-1}	Rate constant for the activity of catechol-*O*-methyltransferase for the catabolism from FDOPA to OMFD.
k_7	min^{-1}	Rate constant for dopamine storage to the vesicle.
k_8	min^{-1}	Rate constant for recycle to cytosolic FDA.
k_9	min^{-1}	Rate constant for metabolism to the acidic metabolites. k_9^{dopac} for FDA to FDOPAC and k_9^{hva} for FDOPAC to FHVA.
k_{11}	min^{-1}	Rate constant for diffusion of the acidic metabolites. k_{11}^{dopac} for FDOPAC and k_{11}^{hva} for FHVA.
V_b	g/ml	Effective blood volume.

TABLE III. Rate constants given in simulation for normal condition

Parameter	Value	Parameter	Value	Parameter	Value
K_1^D	0.0202[a]	k_5	0.000[d]	k_{11}^{dopac}	0.0370[c]
k_2^D	0.0375[a]	k_7	0.0300[c]	k_{11}^{hva}	0.0370[c]
K_1^M	0.0156[b]	k_8	0.0200[c]	V_b	0.0408[a]
k_2^M	0.0391[b]	k_9^{dopac}	0.0170[c]		
k_3	0.0500[a]	k_9^{hva}	0.0272[c]		

Units: g/ml/min (K_1^D, K_1^M), g/ml (V_b), min^{-1} (other parameters).
[a]Values estimated by compartment analysis of monkey striatal TAC [model: two-tissue-four parameters model (Wahl and Nahmias, 1996)].
[b]Values estimated by compartment analysis of monkey cerebellar TAC as well as the previous report (Kumakura et al., 2005).
[c]Values close to the reported value (Cumming and Gjedde, 1998; Cumming et al., 1994; Deep et al., 1997).
[d]We regarded this parameter as negligible as well as the previous studies (Ishikawa et al., 1996; Wahl and Nahmias, 1996).

TAC, which is corrected by tissue OMFD TAC calculated from estimated K_1^M and k_2^M.

k_7 and k_8, which are in the range determined by the previous rat study (Deep et al., 1997), were given, such that simulated standard TAC corresponds to a measured TAC in monkey striatum. Values estimated in ex vivo rat study (Cumming et al., 1994) were given as k_9^{dopac}, k_9^{hva}, k_{11}^{dopac}, k_{11}^{hva}. k_5 were set to zero in simulation.

Values of rate constants given in simulation of the standard TAC are shown in Table III. For the case of the decrease in DDC activity, k_3 was altered between 0.0000 and 0.0500 min^{-1} (between −100 and 0% to the value in Table III). In simulation of the reduction in dopamine storage, k_7 was changed between 0.0000 and 0.0300 min^{-1} (between −100 and 0% to the value in Table III). Similarly, in simulation of the increase in dopamine metabolism to DOPAC, k_9^{dopac} was changed between 0.0170 and 0.0340 min^{-1} (between 0 and +100% to the value in Table III).

Calculation of noisy TACs

Standard deviation (SD) on PET count data in a voxel is in proportion to the inverse of root of noise equivalent count (NEC) as the following equation (Pajevic et al., 1998; Shidahara et al., 2008; Watabe et al., 2000):

$$\frac{\sigma}{C} = \alpha \cdot \frac{1}{\sqrt{\mathrm{NEC}}} \quad (1)$$

where σ is SD on PET count data, C is count in PET image, and α is constant which depends on γ-ray scatter and dead time of detector. α value of PET scanner used in this study was pre-calculated cylinder phantom data (α = 14203.3). NEC data were obtained from actual PET study with a monkey described above. We generated 100 replications of TACs including voxel-level noise from noise-free TACs simulated.

Correction for OMFD

[18F]3-*O*-methyl-FDOPA ([18F]OMFD), the peripheral metabolite of [18F]FDOPA, can cross the blood-brain barrier (BBB) and penetrate the brain tissue. Because [18F]OMFD affects the kinetic analysis, it is necessary to remove [18F]OMFD component from the tissue time-activity curve. The previous analyses (Holden et al., 1997; Martin et al., 1989; Sossi et al., 2001), have assumed uniform diffusion of [18F]OMFD throughout the brain (Doudet et al., 1991), and the contribution of [18F]OMFD was corrected via subtraction of the cerebellum activity from that in a region of interest (e.g., striatum). Note that the cerebellum is taken to be a reference region in which specific binding of [18F]FDOPA is negligible. However, it is acknowledged that the subtraction of the reference region results in overcorrection for [18F]OMFD because some of the reference region activity is attributed to [18F]FDOPA (Kumakura et al., 2005, 2007). To avoid this overcorrection, the [18F]OMFD component in the striatum were calculated from the parameters estimated by compartment analysis of the cerebellar TAC (Kumakura et al., 2005, 2006, 2007).

OMFD component in the simulated TACs were calculated by the following equation, and corrected in all analyses of this study except for Gjedde-Patlak analysis.

$$C_{\mathrm{OMFD}}(t) = K_1^M \int_0^t C_a^M(\tau) e^{-k_2^M (t-\tau)} d\tau \quad (2)$$

K_1^M and k_2^M values estimated from cerebellum TAC as described above. Then, simulated total tissue TACs were corrected by calculated OMFD component. For K_i estimation by Gjedde-Patlak method, OMFD com-

ponent in TACs were corrected via subtraction of the cerebellar TAC in monkey as described previously (Martin et al., 1989).

Data analysis and evaluation of sensitivity

For the Gjedde-Patlak and Logan methods, linear regression analysis proceeded following Eqs. 3 and 4, respectively.

$$\frac{\bar{C}_{\mathrm{PET}}(t)}{C_{\mathrm{a}}^{\mathrm{D}}(t)} = K_{\mathrm{i}} \cdot \frac{\int_0^t C_{\mathrm{a}}^{\mathrm{D}}(\tau)d\tau}{C_{\mathrm{a}}^{\mathrm{D}}(t)} + \text{inter sept} \quad (3)$$

$$\frac{\int_0^t \bar{C}_{\mathrm{PET}}(\tau)d\tau}{C_{\mathrm{PET}}(t)} = V_{\mathrm{T}} \cdot \frac{\int_0^t C_{\mathrm{a}}^{\mathrm{D}}(\tau)d\tau}{C_{\mathrm{PET}}(t)} + \text{inter sept} \quad (4)$$

C_{PET} is defined as total radioactivity minus the OMFD contribution (units: Bq/ml). K_{i} and V_{T} were estimated from the slope in linear regression. In the analysis implementing the Kumakura method, Eq. 5 was used for multilinear regression.

$$\int_0^t \bar{C}_{\mathrm{PET}}(\tau)d\tau = V_{\mathrm{T}} \cdot \int_0^t C_{\mathrm{a}}^{\mathrm{D}}(\tau)d\tau - \frac{\bar{C}_{\mathrm{PET}}(t)}{k_{\mathrm{loss}}} + \frac{V_{\mathrm{f}} + V_{\mathrm{b}}}{k_{\mathrm{loss}}} \cdot C_{\mathrm{a}}^{\mathrm{D}}(t) \quad (5)$$

Three coefficients, V_{T}, $1/k_{\mathrm{loss}}$, $(V_{\mathrm{f}}+V_{\mathrm{b}})/k_{\mathrm{loss}}$, were estimated by multilinear regression. For this analysis, 60–120 min TAC data were employed.

To compare the sensitivity of macro parameters to simulated alterations in [^{18}F]FDOPA kinetics, the percentage difference between macro parameters estimated from TACs with altered k_3, k_7, or k_9^{dopac}, were compared to the same macro parameters estimated from the standard TAC. The percent change was calculated by the following equation.

$$\%\text{change} = \frac{p - p_{\mathrm{std}}}{p_{\mathrm{std}}} \times 100 \quad (6)$$

p and p_{std} were defined as values of parameters estimated from TAC in case of altering k_3, k_7, or k_9^{dopac} and standard TAC, respectively. We regarded %change as the sensitivity to changes in each pathway.

To confirm whether macro parameters can detect the alteration with k_3, k_7, or k_9^{dopac} in noisy case, we examined Welch's t test between macro parameters estimated from altered TACs and standard TACs.

RESULTS

A standard TAC simulated by given rate constants in Table III and metabolite-corrected input functions are shown in Figure 3. The simulated standard TAC nearly corresponded to the measured TAC. TACs in the case of altering k_3, k_7, or k_9^{dopac} are shown in Figure 4. The smaller the k_7 value was, the more rapidly

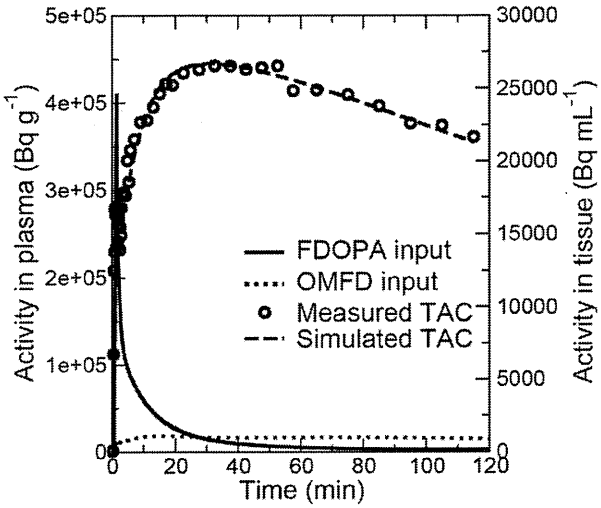

Fig. 3. Input functions and standard TAC as normal condition.

the TAC declined after 50 min post-injection of [^{18}F]FDOPA. Similarly, in the case of increased k_9^{dopac}, a greater reduction of the TAC was observed after 30 min post-injection.

In most of the regression by three conventional methods in both noise-free and noise-added cases, good correlations were observed (correlation coefficients r were ≥ 0.71, ≥ 0.77, and ≥ 0.99 for Gjedde-Patlak, Logan, and Kumakura method, respectively). However, some regression by Gjedde-Patlak analysis to voxel-level noise added data were failed.

Trends of %change calculated from parameters estimated by three methods are shown in Figure 5. In noise-free evaluation, k_{loss} estimated by Kumakura method showed the largest %change to changes in k_7 and k_9^{dopac}. The other macro parameters also change moderately with the changes in k_7 and k_9^{dopac}. For the case of decreasing k_3 from 0.0500 to 0.0100 min^{-1}, the %change of K_{i} and V_{T} were greater than k_{loss}. However, when k_3 was approximately zero, k_{loss} increased quite dramatically.

Addition of voxel-level noise caused large variation and bias of k_{loss}. The changes in k_{loss} estimated from voxel-level noise added data to k_3, k_7 or k_9^{dopac} were not significant ($P > 0.05$), except for the case $k_3 < 0.0250$ min^{-1}. K_{i} and V_{T} were not affected by voxel-level noise. These two parameters changed significantly to the alteration of k_3, k_7, or k_9^{dopac} ($P < 0.05$).

DISCUSSION

Our study aimed to compare the sensitivity of conventional macro parameters to the changes of DDC activity, dopamine storage in the vesicle, and dopamine metabolism to the acidic metabolites. We developed the model with detailed pathways in the dopa-

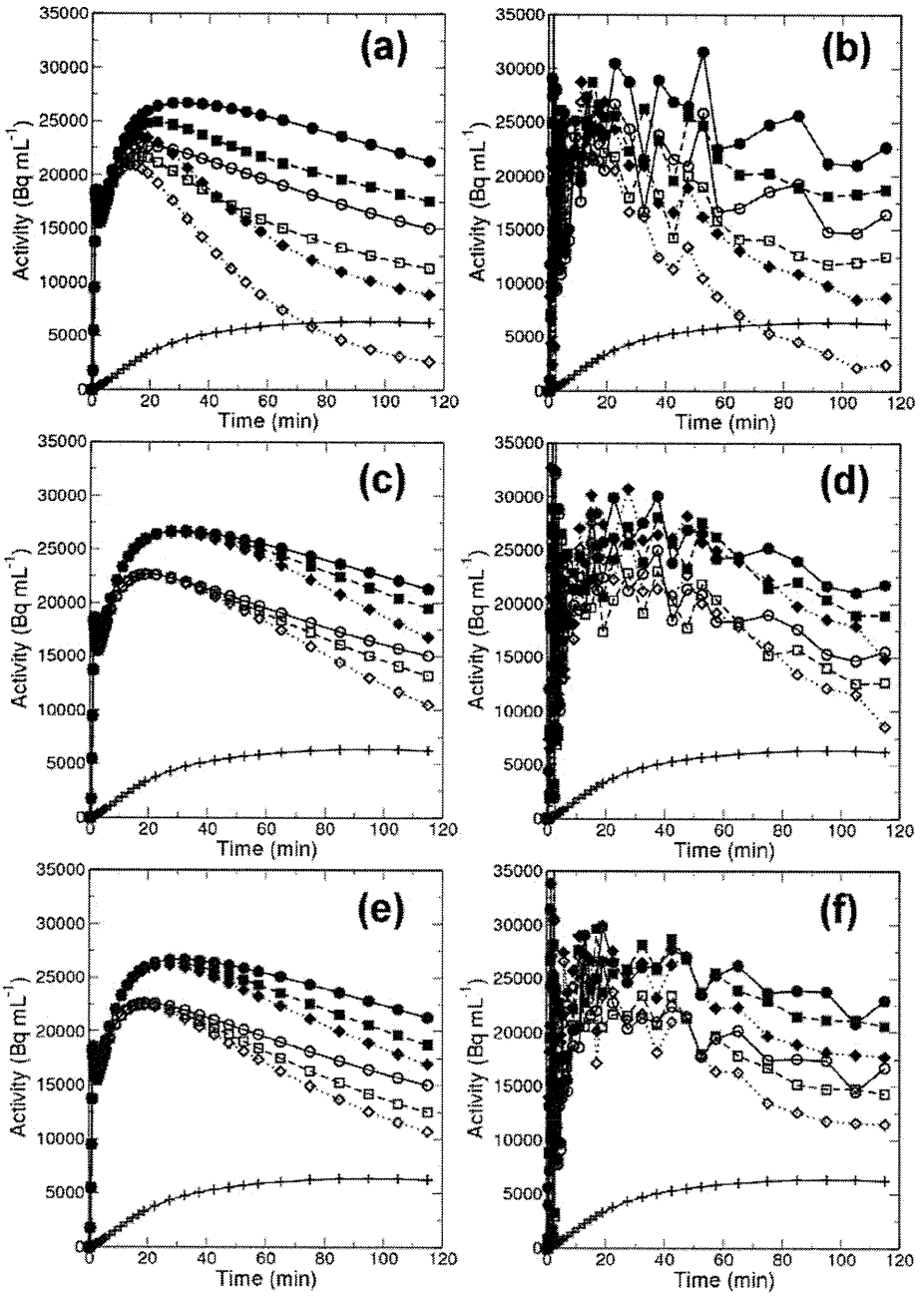

Fig. 4. Simulated TACs in the case of altering k_3 [upper row: (a), (b)], k_7 [middle row: (c), (d)], or k_9^{dopac} [bottom row: (e), (f)]. Noise free or noise added TACs were shown in left column [(a), (c), and (e)] or right column [(b), (d), and (f)], respectively. Legends: closed symbols: simulated TACs, open symbols: TACs corrected for OMFD component, plus symbols: OMFD TACs, solid lines: standard TACs, dashed lines: TACs in case to alter the rate constant by -50% (k_3, k_7) or $+50\%$ (k_9^{dopac}), dotted lines: TACs in case to alter the rate constant by -100% (k_3, k_7) or $+100\%$ (k_9^{dopac}).

mine neuron (DF model) and simulated TACs with changes in DDC activity (k_3), dopamine storage in the vesicle (k_7), and metabolism from dopamine to DOPAC (k_9^{dopac}). Three macro parameters, the net influx of FDOPA (K_i), total distribution volume (V_T), and the rate constants for clearance of the acidic metabolites of FDA from the tissue, k_{loss}, were estimated by three conventional methods with linear least squares algorithm, Gjedde-Patlak graphical analysis (Gjedde, 1981, 1982; Martin et al., 1989; Patlak and Blasberg, 1985; Patlak et al., 1983), Logan graphical analysis, which is popular method in recep-

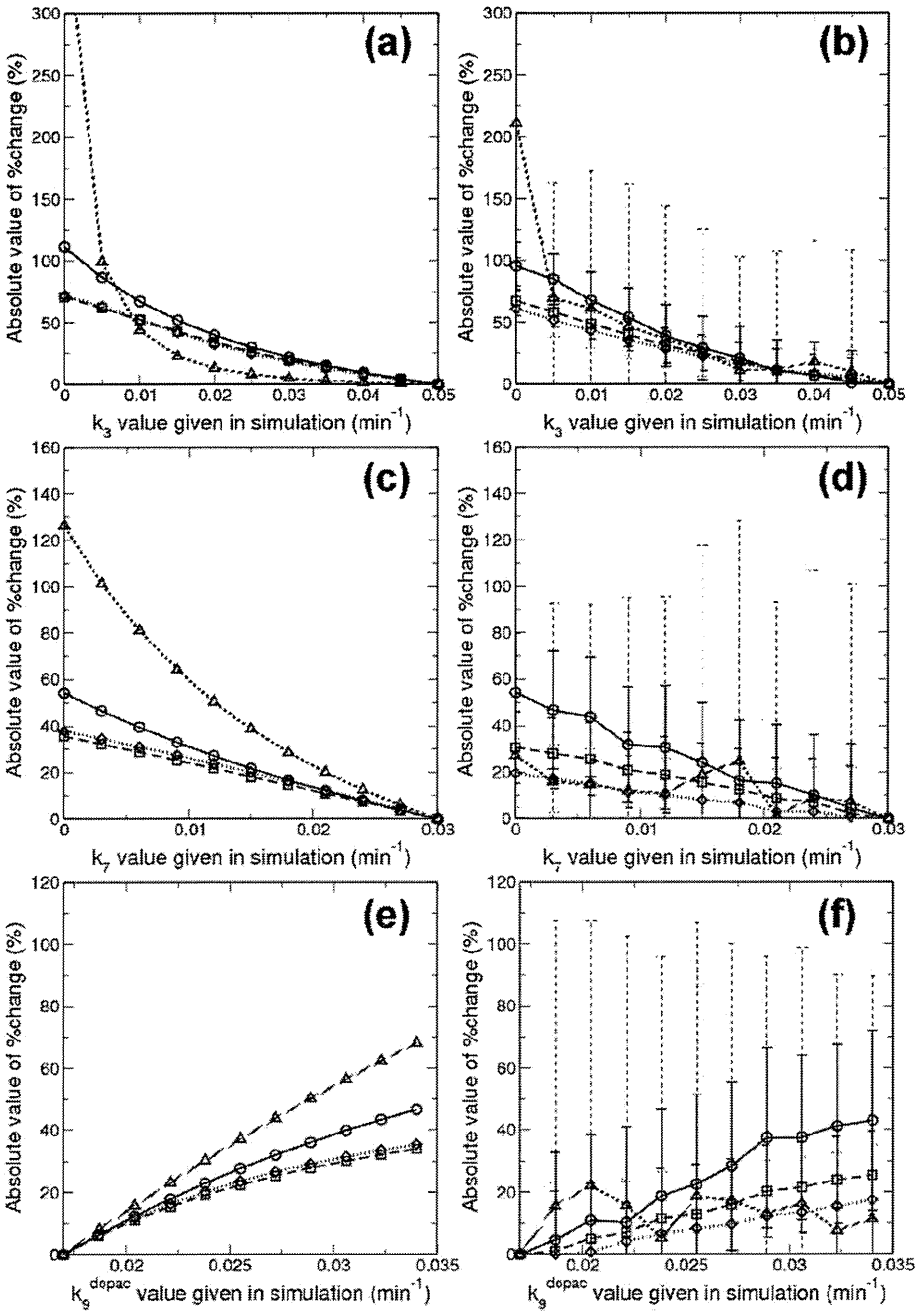

Fig. 5. Trends of percent change in the case of altering k_3 [upper row: (a), (b)], k_7 [middle row: (c), (d)], or k_9^{dopac} [bottom row: (e), (f)]. Noise free or noise added TACs were shown in left column [(a), (c), and (e)] or right column [(b), (d), and (f)], respectively. Legends: circles and solid lines: K_i (Gjedde-Patlak), squares and roughly dashed lines: V_T (Logan), diamonds and dotted lines: V_T (Kumakura), triangle and fine dashed lines: k_{loss} (Kumakura).

tor kinetic study (Kawatsu et al., 2002; Logan et al., 1990) and Kumakura method, which is proposed by Kumakura et al. (Kumakura et al., 2006). In noise-free simulations, k_{loss} estimated by Kumakura method showed the most sensitive to changes in k_7 and k_9^{dopac} among the conventional macro parameters, which suggests that k_{loss} is sensitive to the changes in dopamine storage and metabolism. This finding is in agreement with previous clinical studies (Kumakura et al., 2005, 2006) that show that among the macro parameters estimated by three conventional methods, k_{loss} was differentiated most clearly.

The interpretation of k_{loss} is that it represents the net diffusion of acidic metabolites of FDA, FDOPAC, and FHVA, from brain tissue (Holden et al., 1997; Kumakura et al., 2006; Sossi et al., 2001). Consistent with the definition of k_{loss}, is that it correlated well with the parameter of k_7 and k_9^{dopac} (Ishikawa et al., 1996; Ito et al., 2002; Kumakura et al., 2004; Martin et al., 1989; McGowan et al., 2004; Morrish et al., 1995; Piccini et al., 2005), which are related to washout of FDA and its metabolites from dopaminergic nerve as shown in Figure 2.

In multilinear fitting by Kumakura method, better correlation was observed relative to Patlak or Logan method even if noise were added to the simulated TACs. However, noise in C_{PET} heavily influenced the estimation of k_{loss} and resulted that k_{loss} estimated can not detect the changes in dopamine storage and metabolism significantly. By Kumakura et al., the overestimation of the voxel-wise estimates of k_{loss} was reported (Kumakura et al., 2006). These results and findings suggest voxel-wise estimation may not be optimum for k_{loss} estimation. Note that the voxel-noise was estimated empirically in our simulation. The noise level heavily depends on experimental conditions. For example, we acquired PET data in 2D mode and, the noise level is significantly reduced if we acquired PET data in 3D mode.

The bias of k_{loss} caused by noise can be suppressed by the rearrangement of multilinear equation in Kumakura method (Kumakura et al., 2010a), as described in Appendix. By the rearrangement of Kumakura method, the k_{loss} values were close to ones estimated from noise-free data (see Fig. 6).

K_i and V_T values changed more sensitively than k_{loss} when k_3 was altered between 0.0100 and 0.0500 min^{-1}. And, the changes in both noise added cases were significant. These results suggest that K_i and V_T can detect the changes in DDC activity more sensitively as compared with k_{loss}. However, k_{loss} was increased dramatically in the case that k_3 was reduced extremely (see upper row in Fig. 5) because k_{loss} approached to the [^{18}F]FDOPA efflux (k_2).

Our simulation with noise showed the robustness of the sensitivity of K_i and V_T to the changes in dopamine pathway, suggesting that K_i and V_T may be suitable for voxel-wise estimation in evaluation of DDC activity, dopamine storage, and metabolism with severe noise in PET data. However, by the procedure such as the rearrangement of Kumakura method, the sensitivity of k_{loss} in noisy case can be improved. This finding suggests k_{loss} may be potentially useful for voxel-wise estimation if the voxel-noise are suppressed.

Gjedde-Patlak analysis has been widely applied in the estimation of the net influx of [^{18}F]FDOPA or DDC activity from [^{18}F]FDOPA PET data (Bouilleret et al., 2005; Cheesman et al., 2005; Cumming and Gjedde, 1998; de la Fuente-Fernandez et al., 2000; Hilker et al., 2005; Ishikawa et al., 1996; Ito et al., 2002; Kumakura et al., 2004; Martin et al., 1989; McGowan et al., 2004; Morrish et al., 1995; Piccini et al., 2005). Linear regression in Gjedde-Patlak analysis, which uses only plasma activity data (C_a^D, see Eq. 3) as independent variables, is robust to the noise in PET data. In the present study, higher sensitivity of K_i to the reduction of DDC activity was suggested. Thus, Gjedde-Patlak analysis is adequate for the estimation of DDC activity.

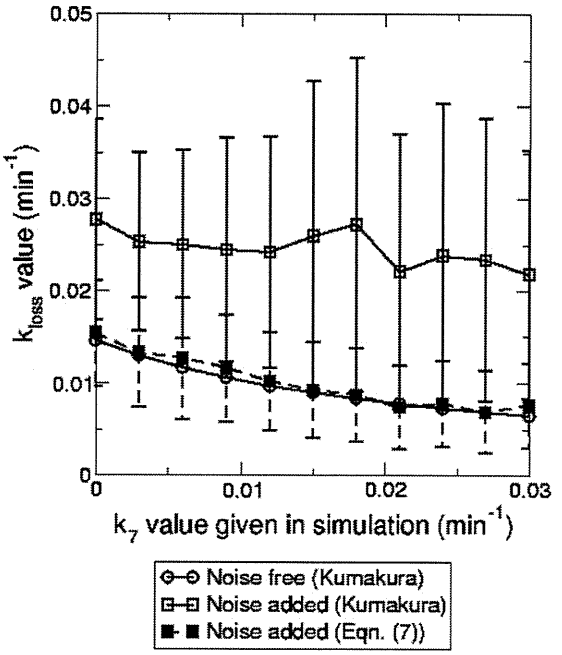

Fig. 6. Comparison trends of estimated k_{loss} between Kumakura method and Eq. 7. By Eq. 7, the bias of k_{loss} was suppressed.

Striatal [^{18}F]FDOPA kinetic is considered as irreversible and Gjedde-Patlak analysis has been applied most popularly in [^{18}F]FDOPA studies (Bouilleret et al., 2005; Cheesman et al., 2005; Cumming and Gjedde, 1998; de la Fuente-Fernandez et al., 2000; Hilker et al., 2005; Ishikawa et al., 1996; Ito et al., 2002; Kumakura et al., 2004; Martin et al., 1989; McGowan et al., 2004; Morrish et al., 1995; Piccini et al., 2005). However, reversible kinetics of [^{18}F]FDOPA was reported in the case of long dynamic PET scan (Holden et al., 1997; Sossi et al., 2001, 2002) and the case that OMFD component was corrected mathematically (Kumakura et al., 2005). Some investigators applied the graphical methods, which assumes the reversible tracer kinetics, for estimations of dopamine turnover and storage capacity (Holden et al., 1997; Kawatsu et al., 2002; Kumakura et al., 2005, 2006; Sossi et al., 2001, 2002). We examined

Logan and Kumakura method as methods for reversible kinetics in this study.

Our simulation model is based on the known dopamine pathway. Several compartment models have been proposed for [^{18}F]FDOPA (Huang et al., 1991; Kuwabara et al., 1993; Wahl and Nahmias, 1996). Deep et al. showed that a model that includes vesicular storage of [^{18}F]FDA, as well as metabolism to [^{18}F]FDOPAC and [^{18}F]FHVA was biologically accurate, based on the agreement between simulated and measured fraction of [^{18}F]FDOPA and its labeled metabolites in rat brain (Deep et al., 1997). A similar model that features both a slow clearing component (vesicular storage) and a fast clearing component ([^{18}F]FDOPA metabolism), and was found to be consistent with the fraction of [^{18}F]FDOPA, [^{18}F]FDOPAC, [^{18}F]FHVA, and [^{18}F]FDA measured in primate (Endres et al., 2004). The DF model used in this study was adapted from the models described above, and those models can be represented by uniting multiple compartments in the DF model. Note that the DF model is quite detailed, and here it is applied to simulate changes in several underlying processes that affect the tracer accumulation in [^{18}F]FDOPA PET studies. Although it is instructive to apply the model for simulations to improve the physiological interpretation of the kinetic macro parameters, the complexity of the DF model makes it unsuitable as a means for parameter estimation.

We simulated TACs that reflect known pathophysiological changes in Parkinson's disease, including the reduction of DDC activity, reduction of dopamine storage in the vesicle, and upregulation of dopamine turnover. Recently, Kumakura et al. suggested that dopamine storage capacity in the Parkinsonian brain is more impaired than is the net FDOPA influx (Kumakura et al., 2006). Chen et al. showed that the binding potential (BP) of [^{11}C]DTBZ, the radiotracer for VMAT2, decreased in a low-dose MPTP monkey and this decrease preceded changes in BP of [^{11}C]raclopride for D2-dopamine receptor and [^{11}C]WIN 35,428 for DAT (Chen et al., 2008). These findings suggest that the reduction of dopamine storage capacity in the vesicle may be a key event in the early phase of Parkinson's disease. According to these findings, and the results in this study, we propose that k_{loss} may be a useful index for early diagnosis of Parkinson's disease.

The upregulation of metabolism to HVA has been also observed in Parkinson's disease (Bernheimer et al., 1973; Hornykiewicz and Kish, 1987). We simulated the TACs with increasing k_9^{hva}, however, it made only a little differences in simulated TACs (data not shown). That suggests that the clearance of [^{18}F]FDA predominantly reflects the clearance of [^{18}F]FDOPAC. As [^{18}F]FDOPAC can clear via two pathways, that is, diffusion into CSF or metabolism to [^{18}F]FHVA, altering the clearance rate of [^{18}F]FHVA alone has minimal effect on the net clearance of [^{18}F]FDA.

In the present simulation, we generated a standard TAC to represent a normal TAC in monkey striatum. The interspecies difference between monkey and human should be considered to better interpret the sensitivity to detect changes in a patient with Parkinson's disease. For example, the clearance of [^{18}F]FDOPA in the plasma of monkey is faster than that in human (Melega et al., 1990). However, estimated k_{loss} values and its trends were close to the ones of normal human control and the patients with Parkinson's disease, resulted in previous human [^{18}F]FDOPA PET study (Kumakura et al., 2006).

We have considered the case of altering only one rate constant in each simulation. However, it is likely that DDC activity, dopamine storage, and metabolism will all be affected in patients with Parkinson's disease. It is necessary to simulate TACs with alteration of the parameters k_3, k_7, and k_9^{dopac} simultaneously for more practical evaluation. To further support our claim in this simulation study, [^{18}F]FDOPA PET experiments using Parkinsonian model animals would be interesting. However, it is clearly out of the scope of the present study.

The DF model could be applied to other physiological and pathological changes that are known to occur in the dopamine system. For example, the reduction of MAO activity in the brain of smokers has been reported (Fowler et al., 1996). For the patients with schizophrenia, the upregulation of DDC activity has been reported (Reith et al., 1994). Moreover, dysfunction of dopamine nerve in the basal ganglia of patients with other neurological disorders, such as epilepsy (Biraben et al., 2004; Bouilleret et al., 2005) and attention deficit hyperactivity disorder (ADHD) (Ludolph et al., 2008), have been reported.

CONCLUSION

For comparison of sensitivity of macro parameters estimated by conventional analyses to changes in DDC activity, dopamine storage and metabolism, we introduced a compartmental model that describes the detailed dopamine pathway (DF model) for simulating striatal TACs as observed in [^{18}F]FDOPA PET study. The present simulation demonstrated that k_{loss} by Kumakura method is relatively sensitive to the reduction of dopamine storage, and acceleration of dopamine metabolism from FDA to FDOPAC, whereas K_i and V_T can detect the reduction of DDC activity. Simulation with the DF model may help in the development of strategies to evaluate [^{18}F]FDOPA PET studies to optimize sensitivity to physiological changes that may occur in Parkinson's disease and the other neurological disorders.

REFERENCES

Bernheimer H, Birkmayer W, Hornykiewicz O, Jellinger K, Seitelberger F. 1973. Brain dopamine and the syndromes of Parkinson and Huntington. Clinical, morphological and neurochemical correlations. J Neurol Sci 20:415–455.

Biraben A, Semah F, Ribeiro M-J, Douaud G, Remy P, Depaulis A. 2004. PET evidence for a role of the basal ganglia in patients with ring chromosome 20 epilepsy. Neurology 63:73–77.

Borght TMV, Sima AA, Kilbourn MR, Desmond TJ, Kuhl DE, Frey KA. 1995. [3H]methoxytetrabenazine: A high specific activity ligand for estimating monoaminergic neuronal integrity. Neuroscience 68:955–962.

Bouilleret V, Semah F, Biraben A, Taussig D, Chassoux F, Syrota A, Ribeiro MJ. 2005. Involvement of the basal ganglia in refractory epilepsy: An 18F-fluoro-L-DOPA PET study using 2 methods of analysis. J Nucl Med 46:540–547.

Brooks D. 2004. Neuroimaging in Parkinson's disease. NeuroRx 1:243–254.

Chan GL, Doudet DJ, Dobko T, Hewitt KA, Schofield P, Pate BD, Ruth TJ. 1995. Routes of administration and effect of carbidopa pretreatment on 6-[18F]-fluoro-L-dopa/PET scans in non-human primates. Life Sci 56:1759–1766.

Cheesman AL, Barker RA, Lewis SJG, Robbins TW, Owen AM, Brooks DJ. 2005. Lateralisation of striatal function: Evidence from [18F]-dopa PET in Parkinson's disease. J Neurol Neurosurg Psychiatr 76:1204–1210.

Chen MK, Kuwabara H, Zhou Y, Adams RJ, Brasic JR, McGlothan JL, Verina T, Burton NC, Alexander M, Kumar A, Wong DF, Guilarte TR. 2008. VMAT2 and dopamine neuron loss in a primate model of Parkinson's disease. J Neurochem 105:78–90.

Cooper JR, Broom FE, Roth RH. 2003. The biochemical basis of neuropharmacology. Oxford University Press, USA. p197–234.

Cumming P, Boyes BE, Martin WRW, Adam M, Grierson J, Ruth T, McGeer EG. 1987. The metabolism of [18F]6-fluoro-L-3,4-dihydroxyphenylalanine in the hooded rat. J Neurochem 48:601–608.

Cumming P, Gjedde A. 1998. Compartmental analysis of dopa decarboxylation in living brain from dynamic positron emission tomograms. Synapse 29:37–61.

Cumming P, Kuwabara H, Gjedde A. 1994. A kinetic analysis of 6-[18F]fluoro-L-dihydroxyphenylalanine metabolism in the rat. J Neurochem 63:1675–1682.

Cumming P, Yokoi F, Chen A, Deep P, Dagher A, Reutens D, Kapczinski F, Wong DF, Gjedde A. 1999. Pharmacokinetics of radiotracers in human plasma during positron emission tomography. Synapse 34:124–134.

de la Fuente-Fernandez R, Pal PK, Vingerhoets FJ, Kishore A, Schulzer M, Mak EK, Ruth TJ, Snow BJ, Calne DB, Stoessl AJ. 2000. Evidence for impaired presynaptic dopamine function in parkinsonian patients with motor fluctuations. J Neural Transm 107:49–57.

Deep P, Gjedde A, Cumming P. 1997. On the accuracy of an [18F]FDOPA compartmental model: Evidence for vesicular storage of [18F]fluorodopamine in vivo. J Neurosci Methods 76:157–165.

Doudet DJ, McLellan CA, Carson R, Adams HR, Miyake H, Aigner TG, Finn RT, Cohen RM. 1991. Distribution and kinetics of 3-*O*-methyl-6-[18F]fluoro-L-dopa in the rhesus monkey brain. J Cereb Blood Flow Metab 11:726–734.

Endres CJ, DeJesus OT, Uno H, Doudet DJ, Nickles RJ, Holden JE. 2004. Time profile of cerebral [18F]6-fluoro-L-dopa metabolites in nonhuman primate: Implications for the kinetics of therapeutic L-dopa. Front Biosci 9:505–512.

Firnau G, Sood S, Chirakal R, Nahmias C, Garnett ES. 1987. Cerebral metabolism of 6-[18f]fluoro-L-3,4-dihydroxyphenylalanine in the primate. J Neurochem 48:1077–1082.

Fowler J, Logan J, Volkow N, Wang G, MacGregor R, Ding Y. 2002. Monoamine oxidase: Radiotracer development and human studies. Methods 27:263–277.

Fowler JS, Volkow ND, Wang GJ, Pappas N, Logan J, MacGregor R, Alexoff D, Shea C, Schlyer D, Wolf AP, Warner D, Zezulkova I, Cilento R. 1996. Inhibition of monoamine oxidase B in the brains of smokers. Nature 379:733–736.

Frey KA, Koeppe RA, Kilbourn MR, Borght TMV, Albin RL, Gilman S, Kuhl DE. 1996. Presynaptic monoaminergic vesicles in Parkinson's disease and normal aging. Ann Neurol 40:873–884.

Gjedde A. 1981. High- and low-affinity transport of D-glucose from blood to brain. J Neurochem 36:1463–1471.

Gjedde A. 1982. Calculation of cerebral glucose phosphorylation from brain uptake of glucose analogs in vivo: A re-examination. Brain Res 257:237–274.

Gjedde A, Leger GC, Cumming P, Yasuhara Y, Evans AC, Guttman M, Kuwabara H. 1993. Striatal L-dopa decarboxylase activity in Parkinson's disease in vivo: Implications for the regulation of dopamine synthesis. J Neurochem 61:1538–1541.

Herzog H, Tellmann L, Hocke C, Pietrzyk U, Casey ME, Kuwert T. 2004. NEMA NU2-2001 guided performance evaluation of four Siemens ECAT PET scanners. IEEE Trans Nucl Sci 51:2662–2669.

Hilker R, Thomas AV, Klein JC, Weisenbach S, Kalbe E, Burghaus L, Jacobs AH, Herholz K, Heiss WD. 2005. Dementia in Parkinson disease: Functional imaging of cholinergic and dopaminergic pathways. Neurology 65:1716–1722.

Holden JE, Doudet D, Endres CJ, Chan GL-Y, Morrison KS, Vingerhoets FJG, Snow BJ, Pate BD, Sossi V, Buckley KR, Ruth TJ. 1997. Graphical analysis of 6-fluoro-L-dopa trapping: Effect of inhibition of catechol-*O*-methyltransferase. J Nucl Med 38:1568–1574.

Hornykiewicz O, Kish SJ. 1987. Biochemical pathophysiology of Parkinson's disease. Adv Neurol 45:19–34.

Huang S, Yu D, Barrio J, Grafton S, Melega W, Hoffman J, Satyamurthy N, Mazziotta J, Phelps M. 1991. Kinetics and modeling of L-6-[18F]fluoro-dopa in human positron emission tomographic studies. J Cereb Blood Flow Metab 11:898–913.

Ishikawa T, Dhawan V, Chaly T, Margouleff C, Robeson W, Dahl JR, Mandel F, Spetsieris P, Eidelberg D. 1996. Clinical significance of striatal DOPA decarboxylase activity in Parkinson's disease. J Nucl Med 37:216–222.

Ito K, Nagano-Saito A, Kato T, Arahata Y, Nakamura A, Kawasumi Y, Hatano K, Abe Y, Yamada T, Kachi T, Brooks DJ. 2002. Striatal and extrastriatal dysfunction in Parkinson's disease with dementia: A 6-[18F]fluoro-L-dopa PET study. Brain 125:1358–1365.

Kawatsu S, Kato T, Nagano-Saito A, Hatano K, Ito K, Ishigaki T. 2002. New insight into the analysis of 6-[18F]fluoro-L-DOPA PET dynamic data in brain tissue without an irreversible compartment: Comparative study of the Patlak and Logan analyses. Radiat Med 21:47–54.

Kudomi N, Choi E, yamamoto S, Watabe H, Kim KM, Shidahara M, Ogawa M, Teramoto N, Sakamoto E, Iida H. 2003. Development of a GSO detector assembly for a continuous blood sampling system. IEEE Trans Nucl Sci 50:70–73.

Kumakura Y, Danielsen EH, Reilhac A, Gjedde A, Cumming P. 2004. Levodopa effect on [18F]fluorodopa influx to brain: Normal volunteers and patients with Parkinson's disease. Acta Neurol Scand 110:188–195.

Kumakura Y, Vernaleken I, Grunder G, Bartenstein P, Gjedde A, Cumming P. 2005. PET studies of net blood-brain clearance of FDOPA to human brain: Age-dependent decline of [18F]fluorodopamine storage capacity. J Cereb Blood Flow Metab 25:807–819.

Kumakura Y, Gjedde A, Danielsen EH, Christensen S, Cumming P. 2006. Dopamine storage capacity in caudate and putamen of patients with early Parkinson's disease: Correlation with asymmetry of motor symptoms. J Cereb Blood Flow Metab 26:358–370.

Kumakura Y, Cumming P, Vernaleken I, Buchholz HG, Siessmeier T, Heinz A, Kienast T, Bartenstein P, Grunder G. 2007. Elevated [18F]fluorodopamine turnover in brain of patients with schizophrenia: An [18F]fluorodopa/positron emission tomography study. J Neurosci 27:8080–8087.

Kumakura Y, Danielsen EH, Gjedde A, Vernaleken I, Buchholz H-G, Heinz A, Gränder G, Bartenstein P, Cumming P. 2010a. Elevated [(18)F]FDOPA utilization in the periaqueductal gray and medial nucleus accumbens of patients with early Parkinson's disease. Neuroimage 49:2933–2939.

Kumakura Y, Vernaleken I, Buchholz H-G, Borghammer P, Danielsen E, Grnder G, Heinz A, Bartenstein P, Cumming P. 2010b. Age-dependent decline of steady state dopamine storage capacity of human brain: An FDOPA PET study. Neurobiol Aging 31:447–463.

Kuwabara H, Cumming P, Reith J, L¥'eg G, Diksic M, Evans A, Gjedde A. 1993. Human striatal L-dopa decarboxylase activity estimated in vivo using 6-[18F]fluoro-dopa and positron emission tomography: Error analysis and application to normal subjects. J Cereb Blood Flow Metab 13:43–56.

Lee CS, Samii A, Sossi V, Ruth TJ, Schulzer M, Holden JE, Wudel J, Pal PK, de la Fuente-Fernandez R, Calne DB, Stoessl AJ. 2000. In vivo positron emission tomographic evidence for compensatory changes in presynaptic dopaminergic nerve terminals in Parkinson's disease. Ann Neurol 47:493–503.

Lloyd K, Hornykiewicz O. 1970. Parkinson's disease: Activity of L-dopa decarboxylase in discrete brain regions. Science 170:1212–1213.

Logan J, Fowler JS, Volkow ND, Wolf AP, Dewey SL, Schlyer DJ, MacGregor RR, Hitzemann R, Bendriem B, Gatley SJ. 1990. Graphical analysis of reversible radioligand binding from time-ac-

tivity measurements applied to [N-^{11}C-methyl]-(-)-cocaine PET studies in human subjects. J Cereb Blood Flow Metab 10:740–747.
Ludolph AG, Kassubek J, Schmeck K, Glaser C, Wunderlich A, Buck AK, Reske SN, Fegert JM, Mottaghy FM. 2008. Dopaminergic dysfunction in attention deficit hyperactivity disorder (ADHD), differences between pharmacologically treated and never treated young adults: A 3,4-dihdroxy-6-[^{18}F]fluorophenyl-L-alanine PET study. Neuroimage 41:718–727.
Martin WR, Palmer MR, Patlak CS, Calne DB. 1989. Nigrostriatal function in humans studied with positron emission tomography. Ann Neurol 26:535–542.
Matsubara K, Watabe H, Hayashi T, Minato K, Iida H. 2010. Evaluation of bias of the influx constant estimated by Patlak analysis for [^{18}F]FDOPA PET: Influence of metabolites for [^{18}F]FDOPA. Seitai-Ikougaku 48:66–74.
McGowan S, Lawrence AD, Sales T, Quested D, Grasby P. 2004. Presynaptic dopaminergic dysfunction in schizophrenia: A positron emission tomographic [^{18}F]fluorodopa study. Arch Gen Psychiatry 61:134–142.
Melega WP, Hoffman JM, Luxen A, Nissenson CHK, Phelps ME, Barrio JR. 1990. The effects of carbidopa on the metabolism of 6-[^{18}F]fluoro-L-dopa in rats, monkeys and humans. Life Sci 47:149–157.
Morrish PK, Sawle GV, Brooks DJ. 1995. Clinical and [^{18}F] dopa PET findings in early Parkinson's disease. J Neurol Neurosurg Psychiatr 59:597–600.
Pajevic S, Daube-Witherspoon ME, Bacharach SL, Carson RE. 1998. Noise characteristics of 3-D and 2-D PET images. IEEE Trans Med Imaging 17:9–23.
Patlak CS, Blasberg RG. 1985. Graphical evaluation of blood-to-brain transfer constants from multiple-time uptake data. Generalizations. J Cereb Blood Flow Metab 5:584–590.
Patlak CS, Blasberg RG, Fenstermacher JD. 1983. Graphical evaluation of blood-to-brain transfer constants from multiple-time uptake data. J Cereb Blood Flow Metab 3:1–7.
Piccini P, Pavese N, Hagell P, Reimer J, Bjorklund A, Oertel WH, Quinn NP, Brooks DJ, Lindvall O. 2005. Factors affecting the clinical outcome after neural transplantation in Parkinson's disease. Brain 128:2977–2986.
Pifl C, Hornykiewicz O. 2006. Dopamine turnover is upregulated in the caudate/putamen of asymptomatic MPTP-treated rhesus monkeys. Neurochem Int 49:519–524.
Reith J, Benkelfat C, Sherwin A, Yasuhara Y, Kuwabara H, Andermann F, Bachneff S, Cumming P, Diksic M, Dyve SE, Etienne P, Evans AC, Lal S, Shevell M, Savard G, Wong DF, Chouinard G, Gjedde A. 1994. Elevated dopa decarboxylase activity in living brain of patients with psychosis. Proc Natl Acad Sci USA 91:11651–11654.
Shidahara M, Watabe H, Kim KM, Kudomi N, Ito H, Iida H. 2008. Optimal scan time of oxygen-15-labeled gas inhalation autoradiographic method for measurement of cerebral oxygen extraction fraction and cerebral oxygen metabolic rate. Ann Nucl Med 22:667–675.
Sossi V, Doudet DJ, Holden JE. 2001. A reversible tracer analysis approach to the study of effective dopamine turnover. J Cereb Blood Flow Metab 21:469–476.
Sossi V, de La Fuente-Fernandez R, Holden JE, Doudet DJ, McKenzie J, Stoessl AJ, Ruth TJ. 2002. Increase in dopamine turnover occurs early in Parkinson's disease: Evidence from a new modeling approach to PET ^{18}F-fluorodopa data. J Cereb Blood Flow Metab 22:232–239.
Sossi V, Holden J, de la Fuente-Fernandez R, Ruth T, Stoessl A. 2003. Effect of dopamine loss and the metabolite 3-*O*-methyl-[^{18}F]fluoro-dopa on the relation between the 18F-fluorodopa tissue input uptake rate constant Kocc and the [^{18}F]fluorodopa plasma input uptake rate constant Ki. J Cereb Blood Flow Metab 23:301–309.
Sossi V, de la Fuente-Fernandez R, Holden JE, Schulzer M, Ruth TJ, Stoessl J. 2004. Changes of dopamine turnover in the progression of Parkinson's disease as measured by positron emission tomography: Their relation to disease-compensatory mechanisms. J Cereb Blood Flow Metab 24:869–876.
Sossi V, de la Fuente-Fernandez R, Schulzer M, Troiano AR, Ruth TJ, Stoessl AJ. 2007. Dopamine transporter relation to dopamine turnover in Parkinson's disease: A positron emission tomography study. Ann Neurol 62:468–474.
Stark H, Woods J, Paul I, Hingorani R. 1981. Direct Fourier reconstruction in computer tomography. IEEE Trans Acoust Speech Signal Processing 29:237–245.
Takagi Y, Takahashi J, Saiki H, Morizane A, Hayashi T, Kishi Y, Fukuda H, Okamoto Y, Koyanagi M, Ideguchi M, Hayashi H, Imazato T, Kawasaki H, Suemori H, Omachi S, Iida H, Itoh N, Nakatsuji N, Sasai Y, Hashimoto N. 2005. Dopaminergic neurons generated from monkey embryonic stem cells function in a Parkinson primate model. J Clin Invest 115:102–109.
Takikawa S, Dhawan V, Chaly T, Robeson W, Dahl R, Zanzi I, Mandel F, Spetsieris P, Eidelberg D. 1994. Input functions for 6-[fluorine-18]fluorodopa quantitation in parkinsonism: Comparative studies and clinical correlations. J Nucl Med 35:955–963.
Wahl L, Nahmias C. 1996. Modeling of fluorine-18-6-fluoro-l-dopa in humans. J Nucl Med 37:432–437.
Watabe H, Endres CJ, Breier A, Schmall B, Eckelman WC, Carson RE. 2000. Measurement of dopamine release with continuous infusion of [^{11}C]raclopride: Optimization and signal-to-noise considerations. J Nucl Med 41:522–530.

APPENDIX: REARRANGED KUMAKURA METHOD

Generally, the noise in TAC can be reduced by the integral. Thus, the noise influences to k_{loss} can be reduced by transposition between C_{PET} and its integral in Eq. 5 as the following (Kumakura et al., 2010a):

$$\bar{C}_{\text{PET}}(t) = V_{\text{T}} \cdot k_{\text{loss}} \cdot \int_0^t C_{\text{a}}^{\text{D}}(\tau)d\tau - k_{\text{loss}} \cdot \int_0^t \bar{C}_{\text{PET}}(\tau)d\tau + (V_{\text{f}} + V_{\text{b}}) \cdot C_{\text{a}}^{\text{D}}(t) \quad (7)$$

This equation can directly and simply obtain k_{loss} from second term parameter estimated by multilinear fitting. It doesn't need additional procedure of estimated parameters, as reverse of second term parameter in Kumakura method.

Original Paper

Cerebrovascular Diseases

Cerebrovasc Dis 2011;32:148–154
DOI: 10.1159/000328652

Received: September 20, 2010
Accepted: April 6, 2011
Published online: July 20, 2011

Differences in Diffusion-Weighted Image and Transesophageal Echocardiographical Findings in Cardiogenic, Paradoxical and Aortogenic Brain Embolism

Shigeru Fujimoto[a, c] Kazunori Toyoda[a] Juro Jinnouchi[c] Masahiro Yasaka[a]
Takanari Kitazono[b] Yasushi Okada[a]

[a]Department of Cerebrovascular Disease, Cerebrovascular Center and Clinical Research Center, National Hospital Organization Kyushu Medical Center, and [b]Department of Medicine and Clinical Science, Graduate School of Medical Sciences, Kyushu University, Fukuoka, and [c]Stroke Center, Nippon Steel Yawata Memorial Hospital, Kitakyushu, Japan

Key Words
Acute stroke diagnosis · Aortic arch atherosclerosis · Cardiac embolism · Diffusion weighted image · Patent foramen ovale · Ultrasound diagnosis

Abstract
Background and Purpose: The purpose of the present study was to clarify the difference in the infarct topography on diffusion-weighted image (DWI) and cardiac and aortic findings on transesophageal echocardiography (TEE) in stroke patients with different embolic sources. ***Methods:*** We studied 270 consecutive patients with acute ischemic stroke who had DWI-documented cortical or subcortical infarcts without significant stenosis of the cerebral arteries. As embolic sources, cardiac diseases, right-to-left shunt diseases and an aortic arch atheroma ≥4.0 mm in thickness were identified using various diagnostic tools including TEE. ***Results:*** Seventy-eight (29%) patients had multiple embolic sources. Large infarcts were common in patients in whom cardiac disease was the only embolic source and uncommon in patients in whom aortic atheroma was the only embolic source ($p < 0.0001$). Vertebrobasilar infarcts were relatively common in patients only having aortic atheromas. Atrial septal aneurysms were more common in patients with a right-to-left shunt than in those with a shunt plus other embolic sources ($p = 0.0036$). Unique characteristics of the arch atheroma (mobile plaque, extension to branches, or ulcer formation; $p < 0.0001$) as well as small or moderate-sized infarcts ($p = 0.0004$) were more common in patients with arch atheromas as the only embolic source than in those with atheromas plus other embolic sources. ***Conclusions:*** Embolic stroke patients often have multiple embolic sources. The present study suggests the possibility that embolic stroke has unique clinical features depending on its source. DWI and TEE findings might be helpful in characterizing cardiogenic, paradoxical and aortogenic brain embolism.

Introduction

In magnetic resonance imaging (MRI) studies for acute-stroke patients, diffusion-weighted imaging (DWI) is indispensable for evaluating recent ischemic lesions, particularly small single or multiple infarcts in the cortex

KARGER
Fax +41 61 306 12 34
E-Mail karger@karger.ch
www.karger.com

1015–9770/11/0322–0148$38.00/0

Accessible online at:
www.karger.com/ced

Shigeru Fujimoto, MD
Department of Cerebrovascular Disease, Nippon Steel Yawata Memorial Hospital
1-1-1 Harunomachi, Yahatahigashi-ku
Kitakyushu 805-8505 (Japan)
Tel. +81 93 671 9605, E-Mail fujimoto.s@ns.yawata-mhp.or.jp

or subcortex, where embolic brain infarction frequently occurs [1, 2].

The medical treatment and clinical course of patients with embolic stroke differ as a function of the embolic sources. In addition to transthoracic echocardiography, electrocardiography, MR angiography, and duplex carotid ultrasonography, transesophageal echocardiography (TEE) is an available screening tool for patients with embolic cerebrovascular events [3, 4]. Previous studies using TEE revealed that an aortic arch atheroma of ≥4 mm in thickness [5–7] and a right-to-left shunt [8, 9], such as a patent foramen ovale (PFO) and a pulmonary arteriovenous fistula, are independent risk factors for embolic stroke. A left atrial spontaneous echo contrast and low flow velocity in the left atrial appendage are also known as indicators for intracardiac thrombus formation [10]. Thus, TEE provided detailed information regarding the embolic sources. An essential problem is that, because multiple embolic sources are simultaneously detected in some stroke patients, we often experience difficulty in identifying which embolic source causes stroke.

The purpose of the present study was to clarify which findings in DWI and TEE could be useful in characterizing cardiogenic, paradoxical and aortogenic brain embolism.

Subjects and Methods

Patients

From May 2002 to February 2005, among 624 consecutive stroke patients, 270 patients with first-ever ischemic stroke within 14 days after symptom onset, who had acute infarcts involving the brain cortex or cerebellum and did not have significant stenotic lesions (≥50% in diameter) in the intracranial or extracranial cerebral arteries prospectively underwent TEE; embolism was the probable etiological mechanism for their stroke. In all the patients, infarcts were identified using DWI; vascular lesions were evaluated using both MR angiography and duplex carotid ultrasonography; cerebral angiography was additionally performed if needed. Symptom duration was not considered for patient inclusion as long as an acute infarct was identified on DWI [11].

Transesophageal Echocardiography

Sources of cardioembolism, right-to-left shunt and aortic atheroma were evaluated in all patients. We used a commercially available real-time two-dimensional echocardiography system (HDI5000, Philips) equipped with a 5.0-MHz phased-array omniplane transesophageal transducer. In addition, electrocardiography, including long-term monitoring and transthoracic echocardiography were performed in order to evaluate heart disease and chronic or intermittent arrhythmia as possible embolic sources.

Cardiac embolic sources were defined in accordance with the Trial of Org 10172 in Acute Stroke Treatment (TOAST) classification of high- and medium-risk sources of cardioembolism except PFO and atrial septal aneurysm (ASA) [12]. Spontaneous echo contrast was defined as a dynamic cloud of low-intensity echoes curling up slowly in the left atrium, and was regarded as a possible cardiac embolic source as well as intracardiac thrombus [13].

Paradoxical embolic sources were right-to-left shunt diseases, including an atrial septal defect, PFO and pulmonary arteriovenous fistula. These right-to-left shunt diseases were diagnosed using the Valsalva contrast method [8, 9]. As a finding suggesting paradoxical embolic sources, an ASA (more than 15 mm in amplitude) was also investigated on the M-mode image. Ultrasonography or venous scintigraphy of the legs was performed to detect deep venous thrombosis when a right-to-left shunt was detected.

An aortic embolic source was an atheroma on the aortic arch ≥4.0 mm in thickness [7], identified using TEE. As findings suggesting an aortic embolic source, a mobile plaque [14], ulceration at the atheroma [15] and extension of the atheroma to the branch origin were also assessed [16]. When the atheromatous plaque extended to the origin of either the innominate artery, left common carotid artery or the left subclavian artery, we defined it as an extending atheroma [16].

Diffusion-Weighted Images

MRI studies including DWI were performed in all patients within 7 days after symptom onset. The MRI apparatus was a 1.5-tesla MR (Siemens) unit with echo planar capability. DWI was performed simultaneously using a multislice, single-shot, spin echo planar imaging sequence. Diffusion gradients were applied in each of the *x*-, *y*-, and *z*-axes with two *b* values (0 and 1,000 s/mm^2). A focal hyperintensity on DWI was defined as an acute infarct. The present study was planned to investigate only patients with a high suspicion of embolic stroke. Patients who had only infarcts supplied by deep perforating arteries of the major cerebral arteries were excluded from the study because they were regarded as having small-artery occlusion or branch atheromatous disease rather than cardiogenic, paradoxical or aortogenic brain embolism. The *site* (right carotid system, left carotid system, vertebrobasilar system and multiple vascular systems, fig. 1e), *multiplicity* (single infarct, fig. 1a–c, and multiple infarcts, fig. 1d, e), and the *maximum size* (one third of the parent cerebral artery territory or more = large; more than 15 mm in diameter and less than one third of the parent cerebral artery territory = moderate, and 15 mm or less in diameter = small; fig. 1a–c, respectively) of infarcts were investigated. DWI findings were evaluated by a neuroradiologist blinded to the clinical symptoms and TEE findings.

Data Analysis

When each patient had only one cardiac, paradoxical or aortogenic embolic source, the source was regarded as a definite cause of brain embolism in that patient. Patients were classified into 5 groups according to identified embolic sources: patients only having a cardiac embolic source (cardiogenic brain embolism group), patients only having a paradoxical embolic source (paradoxical brain embolism group), patients only having an aortic embolic source (aortogenic brain embolism group), patients having more than 1 of the above 3 embolic sources (multiple-source group), and patients without any embolic sources (unknown-source group). Among patients of the multiple-source group, 3 subgroups were additionally distinguished: patients who had a cardiac embolic source belonged to the MC subgroup, those having a paradoxical embolic source, to the MP subgroup, and

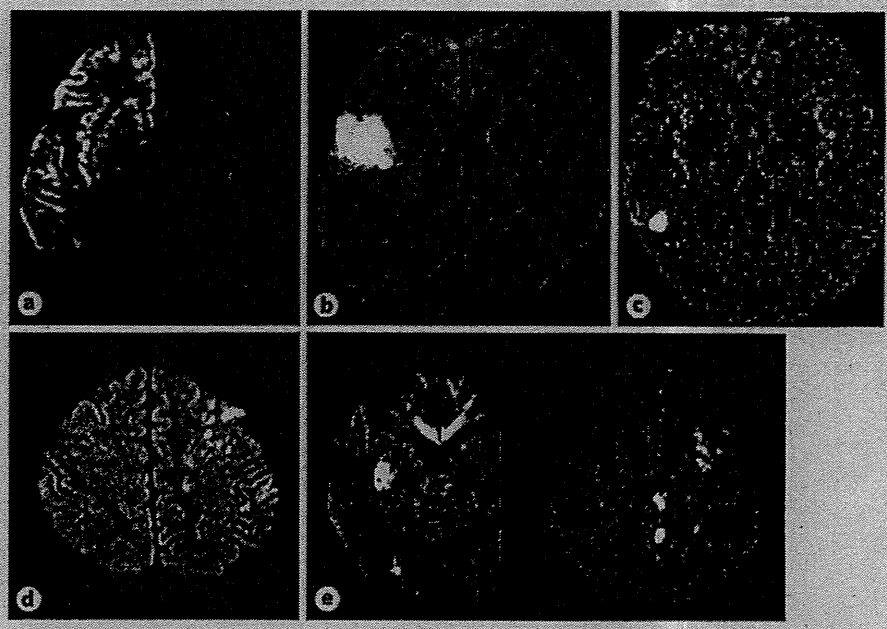

Fig. 1. Acute ischemic lesions on DWI. **a** Acute ischemic lesion of one third of the cerebral artery territory or more. **b** Acute ischemic lesion of more than 15 mm in diameter and less than one third of the cerebral artery territory. **c** Acute ischemic lesion of 15 mm or less in diameter. **d** Acute multiple ischemic lesions within a single cerebral vascular system. **e** Acute multiple ischemic lesions extending to multiple vascular systems.

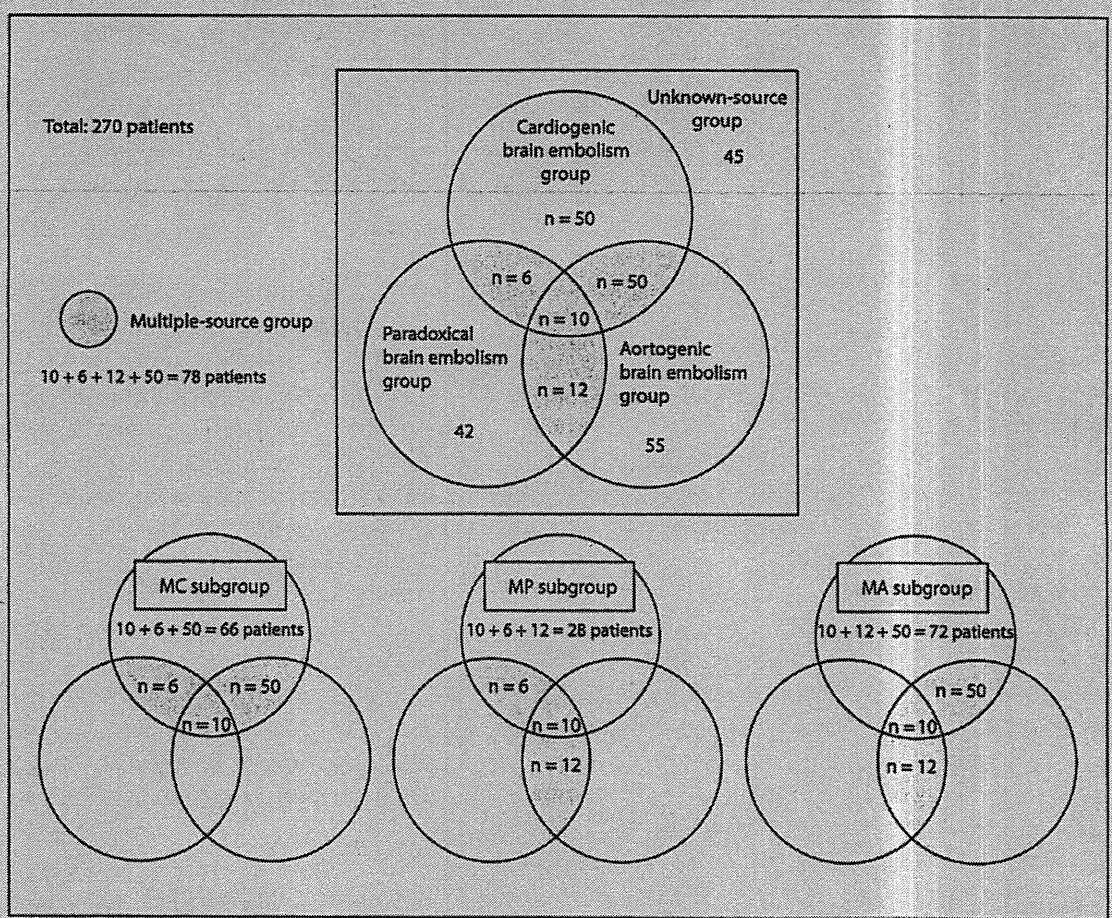

Fig. 2. Number of patients in each group and subgroup.

Table 1. Characteristics of the 5 patient groups

	Cardiogenic (n = 50)	Paradoxical (n = 42)	Aortogenic (n = 55)	Multiple (n = 78)	Unkown (n = 45)	p
Mean age ± SD, years	65.6 ± 11.0	62.0 ± 14.4	68.9 ± 8.9	70.1 ± 9.5	60.7 ± 14.1	<0.0001
Female sex	16 (32%)	18 (43%)	11 (20%)	15 (19%)	18 (40%)	0.0135
Hypertension	30 (60%)	21 (50%)	41 (75%)	56 (72%)	22 (49%)	0.0122
Diabetes mellitus	11 (22%)	10 (24%)	21 (38%)	23 (29%)	7 (16%)	0.1065
Hyperlipidemia	14 (28%)	9 (21%)	23 (42%)	28 (36%)	17 (38%)	0.2241
NIHSS score	3.56 ± 4.30	3.52 ± 4.30	2.18 ± 2.28	4.94 ± 5.34	3.09 ± 3.73	0.0065
Site of lesions						0.0746
Right carotid system	19 (38%)	13 (31%)	9 (16%)	26 (33%)	17 (38%)	
Left carotid system	29 (58%)	18 (43%)	28 (51%)	39 (50%)	22 (49%)	
Vertebrobasilar system	9 (18%)	12 (29%)	24 (44%)	20 (26%)	12 (27%)	
Multiple vascular systems	5 (10%)	1 (2%)	5 (9%)	7 (9%)	5 (11%)	
Border zone lesions	2 (4%)	0 (0%)	0 (0%)	3 (4%)	1 (2%)	0.4227
Hemorrhagic transformation	7 (14%)	1 (2%)	3 (5%)	9 (12%)	0 (0%)	0.0320
Multiple lesions	10 (20%)	13 (31%)	16 (29%)	20 (26%)	11 (24%)	
Size of lesions						<0.0001
Large	18 (36%)	6 (14%)	2 (4%)	23 (29%)	5 (11%)	
Moderate	25 (50%)	20 (48%)	34 (62%)	41 (53%)	20 (44%)	
Small	7 (14%)	16 (38%)	19 (35%)	14 (18%)	20 (44%)	
ASA	3 (6%)	22 (52%)	5 (9%)	8 (10%)	9 (20%)	<0.0001

Size of lesions: large = one third of the parent cerebral artery territory or more; moderate = more than 15 mm in diameter and less than one third of the parent cerebral artery territory; small = 15 mm or less in diameter.

those having an aortic embolic source, to the MA subgroup (fig. 2). The site, multiplicity and size of the acute infarcts on DWI were compared among the 5 groups. Comparison was also performed between the cardiogenic brain embolism group and the MC subgroup, between the paradoxical brain embolism group and the MP subgroup, and between the aortogenic brain embolism group and the MA subgroup. For univariate analysis, the χ^2 test and paired t test were used. A two-tailed probability <0.05 was considered to indicate statistical significance.

Results

Patient Demographics

There were 192 men and 78 women, aged 66.1 ± 11.9 (mean ± SD) years. The National Institute of Health Stroke Scale (NIHSS) scores ranged between 0 and 22 (median 2). Cardiac, paradoxical and aortic embolic sources were detected in 116 (43%), 70 (26%), and 127 (47%) patients, respectively. Fifty patients (19%) belonged to the cardiogenic brain embolism group, 42 (15%) to the paradoxical brain embolism group, 55 (20%) to the aortogenic brain embolism group, 78 (29%) to the multiple-source group, and 45 (16%) to the unknown-source group (fig. 2). Of 78 patients in the multiple-source group, 66 patients belonged to the MC subgroup, 28 to the MP subgroup, and 72 to the MA subgroup.

Characteristics of the 5 Groups (table 1)

Of the baseline characteristics, age ($p < 0.0001$), sex ($p = 0.0135$) and frequency of hypertension ($p = 0.0122$) were different among groups. The site of infarcts tended to be different among groups as well ($p = 0.0746$); in the aortogenic brain embolism group, the infarct was frequent in the vertebrobasilar system, and relatively rare in the right carotid system. Large infarcts were most common in the cardiogenic brain embolism group, and least common in the aortogenic brain embolism group ($p < 0.0001$). Hemorrhagic transformation on computed tomography was most common in the cardiogenic brain embolism group, followed by the multiple-source group ($p = 0.0320$). ASA was most frequently detected in the paradoxical brain embolism group, followed by the unknown-source group ($p < 0.0001$).

Comparison between the Cardiogenic Brain Embolism Group and the MC Subgroup (table 2)

Patients having a cardiac embolic source were divided into 2 groups: those who had (MC subgroup) and those

Table 2. Comparison between the cardiogenic brain embolism group and the MC subgroup

	Cardiogenic (n = 50)	MC subgroup (n = 66)	p
Mean age ± SD, years	65.6 ± 11.0	68.6 ± 8.3	0.1054
Female sex	16 (32%)	15 (23%)	0.1936
Hypertension	30 (60%)	47 (72%)	0.1642
Diabetes mellitus	11 (22%)	20 (31%)	0.2934
Hypercholesterolemia	14 (28%)	21 (32%)	0.6187
NIHSS score	3.56 ± 4.30	5.28 ± 5.57	0.0739
Site of lesions			0.5822
Right carotid system	19 (38%)	19 (29%)	
Left carotid system	29 (58%)	35 (54%)	
Vertebrobasilar system	9 (18%)	16 (25%)	
Multiple vascular systems	5 (10%)	5 (8%)	
Multiple lesions	10 (20%)	15 (23%)	0.6917
Size of lesions			0.9141
Large	18 (36%)	21 (32%)	
Moderate	25 (50%)	34 (52%)	
Small	7 (14%)	10 (15%)	
Hemorrhagic transformation	7 (14%)	8 (12%)	0.5866
Atrial fibrillation	31 (62%)	36 (55%)	0.4757
Intracardiac thrombus	5 (10%)	10 (15%)	0.4596
Spontaneous echo contrast	33 (66%)	50 (77%)	0.1951

Size of lesions: large, moderate and small, as defined in table 1.

Table 3. Comparison between the paradoxical brain embolism group and the MP subgroup

	Paradoxical (n = 42)	MP-subgroup (n = 28)	p
Age, years	62.0 ± 14.4	67.0 ± 9.4	0.1043
Female sex[a]	18 (43%)	4 (14%)	0.0116
Hypertension[a]	21 (50%)	20 (71%)	0.0716
Diabetes mellitus	10 (24%)	8 (29%)	0.6552
Hypercholesterolemia	9 (21%)	9 (32%)	0.3150
NIHSS score	3.52 ± 4.30	3.61 ± 4.18	0.9362
Site of lesions			0.7422
Right carotid system	13 (31%)	8 (29%)	
Left carotid system	18 (43%)	13 (46%)	
Vertebrobasilar system	12 (29%)	9 (32%)	
Multiple vascular systems	1 (2%)	2 (7%)	
Multiple lesions	13 (31%)	6 (21%)	0.3800
Size of lesions			0.3432
Large	6 (14%)	8 (29%)	
Moderate	20 (48%)	11 (39%)	
Small	16 (38%)	9 (32%)	
ASA[a]	22 (52%)	5 (18%)	0.0036
Deep venous thrombosis[b]	12/28 (43%)	3/15 (20%)	0.0899

Size of lesions: large, moderate and small, as defined in table 1.

[a] These variables showed significant differences ($p < 0.1$) and were used for multivariate analysis.

[b] Evaluated using ultrasound in 43 patients.

who did not have (cardiogenic brain embolism group) a paradoxical or aortic embolic source. The underlying clinical and radiological features listed in table 2 were similar in the two groups.

Comparison between the Paradoxical Brain Embolism Group and the MP Subgroup (table 3)

Patients having a paradoxical embolic source were divided into 2 groups: those who had (MP subgroup) and those who did not have (paradoxical brain embolism group) a cardiac or aortic embolic source. The majority of patients in the paradoxical brain embolism group were females ($p = 0.0116$) and more frequently had ASA ($p = 0.0036$) than patients in the MP subgroup.

Comparison between the Aortogenic Brain Embolism Group and the MA Subgroup (table 4)

Patients having an aortic embolic source were divided into 2 groups: those who had (MA subgroup) and those who did not have (aortogenic brain embolism group) a cardiac or paradoxical embolic source. In patients of the aortogenic brain embolism group, admission NIHSS score was lower than in the MA subgroup ($p = 0.0005$). Infarcts in the aortogenic brain embolism group were relatively more common in the vertebrobasilar system, less common in the right carotid system ($p = 0.0527$) and smaller ($p = 0.0004$) than in the MA subgroup. In the aortogenic brain embolism group, an extension of the atheroma to branches was more frequent than in the MA subgroup ($p = 0.0010$), and any of three specific TEE findings on the aortic atheroma, i.e. a mobile plaque, extension to branches, or ulcer formation, was also more frequent ($p < 0.0001$).

Discussion

In the present study, DWI and TEE findings were useful in predicting the etiology of the embolic stroke. The site and size of infarcts were associated with the etiology of brain embolism. The existence of ASA or the special characteristics of aortic arch atheroma, evaluated using

Table 4. Comparison between the aortogenic brain embolism group and the MA subgroup

	Aortogenic (n = 55)	MA subgroup (n = 72)	p
Mean age ± SD, years	68.9 ± 8.9	70.4 ± 9.4	0.9378
Female sex	11 (20%)	14 (19%)	0.3632
Hypertension	41 (75%)	53 (74%)	0.9053
Diabetes mellitus	21 (38%)	22 (31%)	0.3682
Hypercholesterolemia	23 (42%)	26 (36%)	0.5130
NIHSS score	2.18 ± 2.28	4.89 ± 5.27	0.0005
Site of lesions[a]			0.0527
Right carotid system	9 (16%)	25 (35%)	
Left carotid system	28 (51%)	34 (47%)	
Vertebrobasilar system	24 (44%)	20 (28%)	
Multiple vascular systems	5 (9%)	7 (10%)	
Multiple lesions	16 (29%)	20 (28%)	
Size of lesions[a]			0.0004
Large	2 (4%)	20 (28%)	
Moderate	34 (62%)	41 (57%)	
Small	19 (35%)	11 (15%)	
Aortic atheroma ≥4.0 mm			
Mobile plaque	8 (15%)	8 (11%)	0.5633
Extension to branches	39 (71%)	30 (42%)	0.0010
Ulceration	26 (47%)	22 (31%)	0.0542
Any of these 3[a]	47 (85%)	33 (46%)	<0.0001

Size of lesions: large, moderate and small, as defined in table 1.

[a] These variables were significantly different ($p < 0.1$) and were used for multivariate analysis.

TEE, were also useful in distinguishing patients with only a paradoxical or an aortogenic embolic source from those with a paradoxical or aortogenic source plus other embolic sources.

Between patients with a cardiac embolic source plus a right-to-left shunt or aortic atheroma ≥4.0 mm and those with only cardiac embolic sources, there was no significant difference in the patient's background and the characteristics of infarcts. This lack of difference suggests that the etiology in most of patients with both cardiac and extracardiac embolic sources is cardioembolism.

Paradoxical brain embolism is noticed especially in young or cryptogenic stroke patients. In our study, patients with only a paradoxical embolic source were younger and more commonly had ASA than patients in the other groups. A previous study also reported that ASA frequently accompanies PFO [17]. ASA might accelerate right-to-left shunt via PFO. The right-to-left shunt plus ASA might be a diagnostic predictor for paradoxical brain embolism. Sixteen percent of the present patients did not have any embolic sources. One fifth of those patients had ASA, and the frequency was higher than in the other groups. Thus, TEE-undetected right-to-left shunt diseases may be a cause of embolism in such patients.

Aortogenic brain embolism had a peculiarity concerning the site of acute infarcts: it was frequent in the vertebrobasilar system and relatively rare in the right carotid system. Mentel et al. [18] also reported that aortogenic brain embolisms tend to occur in the vertebrobasilar system. Among the 3 major branches of the aortic arch, the left subclavian artery lies in the most distal portion, and this anatomical structure might explain that an embolus from the aortic arch would easily flow into the left subclavian artery. An aortic atheroma with a mobile plaque, extension to branches, or ulcer formation might be a predictor for distinguishing patients only having an aortic embolic source from those having both aortic and extra-aortic embolic sources. Our previous study revealed that both the thickness and the extension of the aortic atheroma were important factors for the occurrence of ischemic stroke [16]. Other previous studies also reported that the presence of ulceration or mobile plaque was associated with embolic stroke [14, 15]. The special characteristics of aortic arch atheromas seem to be significantly associated with the occurrence of aortogenic embolic stroke.

There are several limitations in the present study. We investigated differences between patients with a single embolic source and multiple embolic sources, thus, our findings did not establish the true diagnostic criteria for each embolic pattern. Furthermore, the sample size of each group was too small for multivariate analysis. A prospective study investigating the predictive value of each embolic pattern in a large number of patients is required.

Our study suggests the possibility that embolic stroke has unique clinical features depending on the embolic source. A large infarct might be a positive predictor for cardiogenic brain embolism and might be a negative predictor for aortogenic brain embolism. An infarct in the vertebrobasilar system might be a positive predictor for aortogenic brain embolism. ASA might be an important predictor for paradoxical brain embolism and the special TEE findings on the aortic arch atheroma might be predictors for aortogenic brain embolism. In conclusion, embolic stroke patients often have multiple embolic sources. DWI and TEE findings might be helpful in characterizing cardiogenic, paradoxical and aortogenic brain embolism and in predicting the etiology of acute embolic stroke.

References

1 Yonemura K, Kimura K, Minematsu K, Uchino M, Yamaguchi T: Small centrum ovale infarcts on diffusion-weighted magnetic resonance imaging. Stroke 2002;33: 1541–1544.

2 Warach S, Gaa J, Siewert B, Wielopolski P, Edelman RR: Acute human stroke studied by whole brain echo planar diffusion-weighted magnetic resonance imaging. Ann Neurol 1995;37:231–241.

3 Pop G, Sutherland GR, Koudstaal PJ, Sit TW, de Jong G, Toelandt JRTC: Transesophageal echocardiography in the detection of intracardiac embolic sources in patients with transient ischemic attacks. Stroke 1990;21: 560–565.

4 Cujec B, Polasek P, Voll C, Shuaib A: Transesophageal echocardiography in the detection of potential cardiac sources of embolism in stroke patients. Stroke 1991;22:727–733.

5 Toyoda K, Yasaka M, Nagata S, Yamaguchi T: Aortogenic embolic stroke: a transesophageal echocardiographic approach. Stroke 1992;23:1056–1061

6 Amarenco P, Duyckaerts C, Tzourio C, Henin D, Bousser M-G, Hauw J-J: The prevalence of ulcerated plaques in the aortic arch in patients with stroke. N Engl J Med 1992;326: 221–225

7 Amarenco P, Cohen A, Tzourio C, Bertrand B, Hommel M, Besson G, Chauvel C, Touboul P-J, Bousser M-G: Atherosclerotic disease of the aortic arch and the risk of ischemic stroke. N Engl J Med 1994;331:1474–1479

8 Petty GW, Khandheria BK, Chu CP, Sicks JD, Whisnant JP: Patent foramen ovale in patients with cerebral infarction. A transesophageal echocardiographic study. Arch Neurol 1997;54:819–822.

9 Kristensen B, Malm J, Carlberg B, Stegmayr B, Backman C, Fagerlund M, Olsson T: Epidemiology and etiology of ischemic stroke in young adults aged 18 to 44 years in northern Sweden. Stroke 1997;28:1702–1709.

10 Mugge A, Kuhn H, Nikutta P, Grote J, Lopez JAG, Daniel WG: Assessment of left atrial appendage function by biplane transesophageal echocardiography in patients with nonrheumatic atrial fibrillation: identification of a subgroup of patients at increased embolic risk. J Am Coll Cardiol 1994;23:599–607.

11 Albers GW, Caplan LR, Easton JD, Fayad PB, Mohr JP, Saver JL, Sherman DG: Transient ischemic attack – proposal for a new definition. N Engl J Med 2002;347:1713–1716.

12 Adams HP, Jr, Bendixen BH, Kappelle LJ, Biller J, Love BB, Gordon DL, Marsh EE: 3rd, and the TOAST investigators. Classification of subtype of acute ischemic stroke. Definition for use in a multicenter clinical trial. Stroke 1993;24:35–41.

13 Fatkin D, Herbert E, Feneley MP: Hematologic correlates of spontaneous echo contrast in patients with atrial fibrillation and implications for thromboembolic risk. Am J Cardiol 1994;73:672–676.

14 Ueno Y, Kimura K, Iguchi Y, Shibazaki K, Inoue T, Hattori N, Urabe T: Mobile aortic plaques are a cause of multiple brain infarcts seen on diffusion-weighted imaging. Stroke 2007;38:2470–2476.

15 Stone DA, Hawke MW, LaMonte M, Kittner SJ, Acosta J, Corretti M, Sample C, Price TR, Plotnick GD: Ulcerated atherothrombotic plaques in thoracic aorta are associated with cryptogenic stroke: a multiplane transesophageal echocardiographic study. Am Heart J 1995;130:105–108.

16 Fujimoto S, Yasaka M, Otsubo R, Oe H, Nagatsuka K, Minematsu K: Aortic arch atherosclerotic lesions and the recurrence of ischemic stroke. Stroke 2004;35:1426–1429.

17 Mugge A, Daniel WG, Angermann C, Spes C, Khandheria BK, Kronzon I, Freedberg RS, Keren A, Dennig K, Engberding R, Sutherland GR, Vered Z, Erbel R, Visser CA, Lindert O, Hausmann D, Wenzlaff P: Atrial septal aneurysm in adult patients: a multicenter study using transesophageal echocardiography. Circulation 1995;91:2785–2792.

18 Mentel T, Pasierski T, Szwed H, Baranska-Gieruszczak M, Czlonkowska A: Transesophageal echocardiographic findings in patients with anterior and posterior circulation infarcts. Acta Neurol Scand 1998;97:63–67.

bjh research paper

Prospective multicentre cohort study of heparin-induced thrombocytopenia in acute ischaemic stroke patients

Hiroyuki Kawano,[1,2] Haruko Yamamoto,[3] Shigeki Miyata,[4] Manabu Izumi,[5] Teruyuki Hirano,[2] Naomi Toratani,[6] Isami Kakutani,[4] Jo-Ann I. Sheppard,[7] Theodore E. Warkentin,[7] Akiko Kada,[3] Shoichiro Sato,[6] Sadahisa Okamoto,[2] Kazuyuki Nagatsuka,[6] Hiroaki Naritomi,[6] Kazunori Toyoda,[6] Makoto Uchino[2] and Kazuo Minematsu[6]

[1]Department of Cerebrovascular Medicine, National Cerebral and Cardiovascular Centre, Suita, Osaka, [2]Department of Neurology, Faculty of Life Sciences, Kumamoto University, Kumamoto, [3]Department of Advanced Medical Technology Development, National Cerebral and Cardiovascular Centre, [4]Divisions of Clinical Laboratory and Transfusion Medicine, National Cerebral and Cardiovascular Centre, Suita, Osaka, [5]Division of Cardiology, Department of Internal Medicine, Research Institute for Brain and Blood Vessels Akita, Akita, [6]Department of Neurology, National Cerebral and Cardiovascular Centre, Suita, Osaka, Japan, and [7]Department of Pathology and Molecular Medicine, McMaster University, Hamilton, ON, Canada

Received 10 March 2011; accepted for publication 15 May 2011

Correspondence: Haruko Yamamoto, Department of Advanced Medical Technology Development, National Cerebral and Cardiovascular Centre, 5-7-1 Fujishirodai, Suita, Osaka 565-8565, Japan.
E-mail: harukoya@hsp.ncvc.go.jp

Summary

Acute ischaemic stroke patients sometimes receive heparin for treatment and/or prophylaxis of thromboembolic complications. This study was designed to elucidate the incidence and clinical features of heparin-induced thrombocytopenia (HIT) in acute stroke patients treated with heparin. We conducted a prospective multicentre cohort study of 267 patients who were admitted to three stroke centres within 7 d after stroke onset. We examined clinical data until discharge and collected blood samples on days 1 and 14 of hospitalization to test anti-platelet factor 4/heparin antibodies (anti-PF4/H Abs) using an enzyme-linked immunosorbent assay (ELISA); platelet-activating antibodies were identified by serotonin-release assay (SRA). Patients with a 4Ts score ≥4 points, positive-ELISA, and positive-SRA were diagnosed as definite HIT. Heparin was administered to 172 patients (64·4%: heparin group). Anti-PF4/H Abs were detected by ELISA in 22 cases (12·8%) in the heparin group. Seven patients had 4Ts ≥ 4 points. Among them, three patients (1·7% overall) were also positive by both ELISA and SRA. National Institutes of Health Stroke Scale score on admission was high (range, 16–23) and in-hospital mortality was very high (66·7%) in definite HIT patients. In this study, the incidence of definite HIT in acute ischaemic stroke patients treated with heparin was 1·7% (95% confidence interval: 0·4–5·0). The clinical severity and outcome of definite HIT were unfavourable.

Keywords: acute stroke care, anticoagulation, heparin, platelet, thrombocytopenia.

Immune-mediated heparin-induced thrombocytopenia (HIT), which is caused by platelet-activating IgG antibodies that recognize platelet factor 4 bound to heparin (anti-PF4/heparin Abs), is a relatively common side effect of heparin therapy and presents a strong risk factor for thromboembolic events associated with high mortality and morbidity (Warkentin, 2007a). Prospective studies in Western countries have shown that the prevalence of HIT is 0·3–5% of patients treated with unfractionated heparin (UFH), which varies depending on the clinical settings (Warkentin *et al*, 1995, 2000; Kappers-Klunne

First published online 14 June 2011
doi:10.1111/j.1365-2141.2011.08775.x

et al, 1997). Thrombotic complications occur in approximately one-third to one-half of HIT patients (Warkentin, 2007a). On the other hand, some studies of UFH therapy for acute stroke reported no cases of HIT (Toth & Voll, 2002; Camerlingo *et al*, 2005). To elucidate the prevalence of HIT in acute ischaemic stroke patients who were treated with heparin, we organized a prospective multicentre cohort study that included systematic collection of blood for detection of the antibodies that cause HIT.

Some clinical guidelines do not recommend prescribing heparin in acute ischaemic stroke, and others recommend it mainly for the prevention of deep vein thrombosis (DVT) and pulmonary embolism (PE) (Albers *et al*, 2004; Cardiovascular Disease Educational and Research Trust, 2006; Adams *et al*, 2007). At the participating stroke centres in our study, in addition to the prevention of DVT and PE, UFH is given during the acute phase of ischaemic stroke to the following: patients with emboligenic heart disease or superimposed thrombi on the carotid plaque to prevent embolic complications; patients with particular stroke aetiologies, including cerebral arterial dissection and vasculitis; and patients with embolic stroke of unknown origin until the presence of heart disease is excluded by the results of prolonged electrocardiography and transesophageal echocardiography (Caplan, 2003).

In a previous study of 137 stroke patients who were treated with UFH, 21 patients (15·3%) developed thrombocytopenia (≥40% fall in platelet counts) during or after heparin therapy, and five of these 21 patients had an additional ischaemic stroke (Ramirez-Lassepas *et al*, 1984). A recent study of 200 neurological patients treated with UFH for at least 5 d, including 102 patients with cerebrovascular disorders, demonstrated that 41 patients (20·5%) had anti-PF4/heparin Abs and 5 (2·5%) developed HIT, when the serological diagnosis was made from the presence of antibodies detected by an enzyme-linked immunosorbent assay (ELISA) (Harbrecht *et al*, 2004).

Only a few studies have investigated the prevalence of HIT in acute stroke patients receiving UFH, especially in the Asian population (Kawano *et al*, 2008). In our previous retrospective report of acute ischaemic stroke patients who were treated with UFH, 0·5% of the patients developed HIT diagnosed by both the clinical scoring systems and the serological assays, including ^{14}C-serotonin release assay (SRA) (Kawano *et al*, 2008). However, our retrospective study assessing the prevalence of HIT was limited by the fact that was that antibodies were not assayed in all patients. This limitation may cause an under diagnosis of HIT.

Thus, we performed this prospective multicentre cohort study in 267 patients to determine a more accurate incidence of HIT in patients with acute ischaemic stroke and to elucidate the clinical features of HIT.

Methods

Study design

A prospective multicentre cohort study.

Subjects and settings

This study was conducted in three Japanese stroke centres at the then National Cardiovascular Centre (currently the National Cerebral and Cardiovascular Centre, Osaka), Research Institute for Brain and Blood Vessels Akita (Akita), and Kumamoto University (Kumamoto). Between October 2006 and May 2007, all consecutive patients who met the following criteria were enrolled. Eligible patients were 20 years of age or older and admitted within 7 d after the onset of acute ischaemic stroke, including cerebral infarction and transient ischaemic attack. Patients were excluded for any of the following: (i) active infectious endocarditis, (ii) urgent neurosurgery or cardiovascular surgery would be required, (iii) chronic thrombocytopenia (defined as a platelet count $<100 \times 10^9$/l for more than 30 d), (iv) haematopoietic malignancy and (v) an ongoing need for an anticancer-drug treatment. The study was approved by the research ethics committee of each centre. Heparin therapy was provided to a number of patients depending on the physician's decision (mainly considering the type of stroke and/or the patient's clinical status as described in the Introduction.)

Evaluation

The following patient characteristics were obtained: age, sex, height, body weight, body-mass index, modified Rankin Scale (mRS) score (van Swieten *et al*, 1988) before stroke onset, vascular risk factors (hypertension, diabetes mellitus, dyslipidaemia, current and past smoking habits, drinking habit, including occasional drinking), past history (autoimmune disease, haemodialysis, renal dysfunction, angina, myocardial infarction, cerebral infarction, transient ischaemic attack, pulmonary thromboembolism, extremity gangrene, amputation of an extremity, angiography, heparin exposure, surgical procedure and HIT), platelet counts, antiplatelet/anticoagulant drug use and blood transfusions. The timing and period of heparin administration (including heparin flushes), changes in platelet count, and alternative anticoagulant therapy for HIT (if given) were also examined. Other risk factors for stroke, such as emboligenic heart diseases including atrial fibrillation, were assessed based on the criteria from the Trial of Org 10172 in Acute Stroke Treatment (TOAST) study (Adams *et al*, 1993). Based on the neurological, radiological, cardiological and haematological profiles, the stroke subtype was determined according to the TOAST subtype classification system by a consensus of stroke neurologists. The neurological severity of each patient was assessed by an experienced stroke neurologist according to the National Institutes of Health Stroke Scale (NIHSS) score (Lyden *et al*, 1994) on admission and discharge, and at 3 months after onset. Patient global outcome was also assessed with mRS (van Swieten *et al*, 1988).

Clinical evaluation. The clinical probability of HIT was assessed using the 4Ts scoring system (Warkentin & Heddle, 2003), which is composed of four clinical features that are

given scores of 0, 1, or 2; magnitude of thrombocytopenia; timing of platelet count fall (in relation to heparin therapy); thrombosis or other sequelae; and presence of other explanations for thrombocytopenia. The case reports of the patients, filled out by their physicians, were assessed independently in a blinded fashion by the external Data Assessment Committee, which consisted of two stroke neurologists, according to the 4Ts scoring system after the patient follow-up was completed. If the judgment was not concordant between the two stroke neurologists, they discussed the cases to reach a final consensus and decision. Based on the 4Ts score, the estimated pretest probabilities of HIT were categorized into three groups: low (0–3), intermediate (4–5) and high (6–8) scores. We diagnosed the patients with an intermediate or a high score as 'potential HIT' and those with a low score as 'clinical non-HIT'. These objective assessments for the clinical probability of HIT were done after the patient follow-up was completed as described above, so that no results influenced clinical management. Therefore, some patients were ultimately diagnosed as HIT even though the physicians in charge did not suspect HIT as described in details in the Results section.

Serological evaluation. Blood samples were collected from all patients on the first (to the third) and 14th (±4) hospital days to be tested for anti-PF4/heparin Abs using ELISA (Asserachrom HPIA; Diagnostica Stago, Asnieres, France). The assays were performed in a blinded fashion after patient follow-up was completed. ELISA was performed according to the manufacturer's instructions. The titres of the samples were expressed as values of optical density (OD). The result was considered positive when the titre was greater than the cut-off value, which was determined using the reference control for each kit. To confirm the diagnosis of HIT, SRA was measured for all patients with a positive ELISA and/or ≥4 points in the 4Ts scoring system (n = 29). In addition, samples from 39 patients selected randomly from among all the patients were tested by SRA as a control. Samples were measured as described elsewhere at the Platelet Immunology Laboratory, McMaster University (Hamilton, ON, Canada) blinded to all clinical, platelet count and serological data (Warkentin *et al*, 1992). Any sample that produced ≥10% mean serotonin release with <10% release in the presence of high heparin (at a final concentration of 100 u/ml) and the anti-FcγRIIa monoclonal antibody (IV.3) was considered SRA-positive.

Diagnosis

Based on the results of both the 4Ts clinical score and the serological assays, patients were categorized into four groups as follows: (i) definite HIT (4Ts score ≥4 points with positive results in both ELISA and SRA), (ii) possible HIT (4Ts score ≥4 points with positive result in either ELISA or SRA) and (iii) clinically suspected HIT (4Ts score ≥4 points with negative results in both ELISA and SRA), seropositive status (4Ts score <4 points with positive in both ELISA and SRA). The remaining patients were categorized as HIT unlikely.

Statistical analysis

The variables between the groups of patients treated with and without heparin were compared using Fisher's exact test and the Wilcoxon test. For NIHSS, the change, NIHSS score at discharge minus that at admission, was also determined. Statistical analyses were performed using SAS software version 9.1 (SAS Institute Inc, Cary, NC, USA).

Results

Patient characteristics

A total of 267 patients (mean age 71·7 years; 66·2% men), who were admitted to three stroke centres within 7 d after stroke onset during a 6-month period, were enrolled. Intravenous UFH was administered to 172 patients (64·4%: heparin group) (Fig 1). Male gender, atrial fibrillation, previous ischaemic heart disease, history of surgery using UFH, and history of intra-arterial catheter procedures were significantly more common in patients treated with than without UFH (Table IA). In regard to stroke subtype, large artery atherosclerosis and cardioembolism were more frequent in patients treated with UFH, and small vessel occlusion was more frequent in those without UFH treatment. There was no significant difference in the history of antiplatelet drug use before admission between the patients treated with (66 cases, 38·4%) and without UFH (32 cases, 33·7%) (P = 0·508) (Table IA). Both the NIHSS score at discharge (median, 2 vs. 1, P = 0·020) and mRS at 3 months after stroke onset (median, 2 vs. 1, P < 0·001) were higher in patients treated with UFH (Table IB).

The incidence of HIT

Anti-PF4/heparin Abs were detected at any time point in 22 patients (12·8%) in the heparin group and in 3 (3·2%) of 95 patients who did not receive intravenous UFH respectively (Fig 1), and the difference was significant (P = 0·008). Seven patients (4·1%) were diagnosed as having potential HIT according to the 4Ts score (≥4 points). All seven patients had intermediate scores. Among them, three showed positive results in both ELISA and SRA, to give an incidence of definite HIT of 1·7% [95% confidence interval (CI): 0·4–5·0]. Possible HIT, clinically suspected HIT, and seropositive status were 0%, 2·3% (n = 4), and 2·3% (n = 4), respectively (Fig 1). Of the 95 patients with a positive ELISA who did not receive heparin within 3 months before admission and/or during hospitalization, three were SRA-negative. The OD values of anti-PF4/heparin Abs detected by ELISA seemed a little higher in definite HIT patients than the seropositive status group, although statistical analysis was not performed because of the

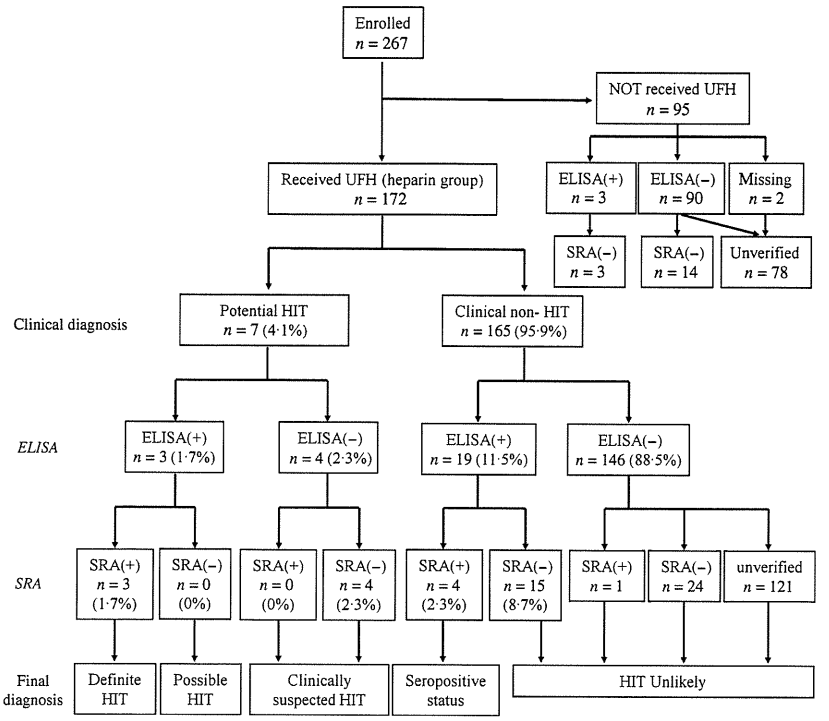

Fig 1. Flow chart for diagnosis of heparin-induced thrombocytopenia. HIT, heparin-induced thrombocytopenia; UFH, unfractionated heparin; ELISA, enzyme-linked immunosorbent assay; SRA, serotonin-release assay.

small sample size (Table II). OD values in ELISA did not correlate with the mean percentage release in SRA (Fig 2). However, the proportion of samples with positive-SRA to those with negative-SRA was greater in the samples with ≥1·5 OD value in ELISA as compared to those with <1·5 OD value. The prevalence of positive-ELISA was not significantly different between patients who received UFH for five or more days (15·9%) and for <5 d (11·4%).

Clinical course and the treatment of definite HIT patients

Only one (Case 3) of three definite HIT patients was suspected of having HIT by the treating physician. This patient had atrial fibrillation and an infarct in the right anterior and middle cerebral arteries. The admission NIHSS score was 17 (Table II). The patient's platelet count decreased from 156 to 99×10^9/l (approximately a 37% fall) in the typical HIT window (5–10 d) and recovered to 227×10^9/l soon after stopping heparin administration on day 7 due to the suspicion of HIT. The patient had a further fall in platelet count, from 227 to 99×10^9/l (approximately a 56% fall), after day 10 with a high OD value (2·086) in ELISA and a weak positive SRA (11% release) (Table II). The patient died due to deterioration from an underlying stroke. The very weak SRA, which was performed during the second platelet count fall, argues somewhat against this patient having HIT. However, HIT antibodies sometimes become weaker very quickly (Warkentin & Kelton, 2001; Greinacher *et al*, 2009), and so it is possible that the SRA would have been stronger during the first platelet count fall.

The other two patients (Cases 1 and 2) that ultimately met the criteria for definite HIT in this study were not suspected of having HIT by their physicians. One patient (Case 1) experienced a stroke of other determined aetiology due to arterial dissection in the intracranial left vertebral artery. The admission NIHSS score was 23 (Table II). The patient had bilateral cerebellar and brain stem infarcts. UFH was administrated for 7 d, and UFH flushes for intravascular catheter were continued for an additional 4 d. The patient showed a 52·0% decrease in platelet count, from 331 to 107×10^9/l, that began on day 5 of heparin with relatively high values in SRA (63·9% release) and ELISA (2·271 OD value) (Table II). Death occurred from stroke on day 11. The other patient (Case 2) with a previous history of recent transient ischaemic attacks had a cardioembolic stroke due to atrial fibrillation 9 d after urgent hemiarch replacement due to aortic dissection. The admission NIHSS score was 16. The patient's platelet count declined from 436 to 286×10^9/l (a drop of approximately 34%) during the typical HIT window of days 5–10 with relatively high values in SRA (51·6% release) and ELISA (1·725 OD value); although the platelet count evolution may be explained by a platelet count profile of post-cardiovascular surgery with cardiopulmonary bypass overshooting around postoperative day 14 and returning gradually to the baseline (Table II). The patient was dependent at discharge and at 3-month follow-up.